TECHNICAL NOTE

D-1603

EXPERIMENTAL INVESTIGATION OF BLAST LOADING ON AN AIRFOIL IN MACH NUMBER 0.7 AIRFLOW WITH INITIAL ANGLE-OF-ATTACK CHANGE OF 20°

By Harold B. Pierce and James C. Manning

Langley Research Center
Langley Station, Hampton, Va.

NATIONAL AERONAUTICS AND SPACE ADMINISTRATION
WASHINGTON

February 1963

Code 1

SINGLE COPY ONLY

NATIONAL AERONAUTICS AND SPACE ADMINISTRATION

TECHNICAL NOTE D-1603

EXPERIMENTAL INVESTIGATION OF BLAST LOADING ON AN AIRFOIL IN MACH NUMBER 0.7 AIRFLOW WITH INITIAL ANGLE-OF-ATTACK CHANGE OF 20°

By Harold B. Pierce and James C. Manning

SUMMARY

An experimental investigation has been completed on the blast loading imposed on an airfoil in Mach number 0.7 flow by a blast wave which caused an initial angle-of-attack change of approximately 20°. Pressure distributions along one chord of the airfoil at intervals of 0.1 millisecond show the initial diffraction of the blast wave around the airfoil while subsequent distributions at intervals of 0.5 millisecond show the progress along the chord of a leading-edge vortex formed in the diffraction period. Normal-force coefficients obtained from the blast test pressure distributions were substantially greater than those from wind-tunnel tests for a period of 10 milliseconds after blast-wave arrival. The investigation, the first conducted at the NASA Ground Blast Apparatus, consisted of two tests made under essentially the same conditions.

INTRODUCTION

Information on blast loading of aircraft is important in the avoidance of damage to an aircraft delivering nuclear weapons and, conversely, in determining the lethal envelope about an aircraft when the blast wave of a nuclear device is to be used as an antiaircraft weapon. Substantial progress, both analytical and experimental, has been made in providing information for the delivery condition, primarily because the aerodynamics lie in the linear range and because full-scale testing is practical and successful. Very little progress has been made in determining the loadings for the antiaircraft problem. The blast wave for antiaircraft purposes is obviously much more intense than that expected in the delivery problem. Vortices are formed as the blast wave diffracts around the airfoil surfaces and the particle velocity in the blast wave increases the angle of attack of the airfoil well beyond the steady-state stall angle. Under such complex conditions, a useful analytical determination of these loadings is unlikely at the present state of knowledge.

An experimental investigation of blast loading in the antiaircraft regime has been conducted by the National Aeronautics and Space Administration. The initial investigations were made at low speed with airplane models in free flight

subjected to blast waves from explosives. The loads were measured in the form of pressure distributions telemetered to a ground-receiving station and the major results are reported in references 1 to 3. Small-scale schlieren studies of the low-speed blast tests were made to corroborate the existence of the traveling vortex deduced from the pressure results of reference 1 and these results are also included in reference 3. The simulation technique employed for the schlieren studies was to immerse an airfoil in a stream of air and strike it with a scaled blast wave originating outside the stream. Reference 4 presents the results of an investigation which used a shock-tube simulation of the blast loading process and extended the speed range to a Mach number of 1.0. The experimental results were shown to be in good agreement with a modified traveling-gust theory. Still another method of simulating blast loading on aircraft is the rocket-sled technique used in the investigation described in reference 5.

Although the free-flight technique yielded adequate results at low speed, it became apparent that the limited frequency response of the telemetering system could not be improved sufficiently for this technique to be practical for an investigation of the loadings at high subsonic speeds. The shock-tube technique of reference 4 would be difficult to use with the larger models required for direct pressure distribution measurements and the accuracy of simulation is believed to suffer from the lack of initial flow over the model. The rocket-sled technique can use a large model and provides an accurate simulation of full-scale conditions. The vibrations of the moving sled, however, provide a hostile environment for the operation of known available high-response pressure instrumentation.

In order to avoid the difficulties of the free-flight, shock-tube, and rocket-sled testing techniques, the NASA adapted the technique used in the small-scale low-speed schlieren studies of reference 3 by using a shock tunnel to provide a flow of high-subsonic speed over the stationary model. While the model is immersed in the flow it is struck by a blast wave and pressure distribution measurements are made. The equipment to provide the test conditions, together with the associated special instrumentation, was located at the NASA Wallops Station and called the NASA Ground Blast Apparatus. Concurrently with the development of the Ground Blast Apparatus, a small-scale model of the Ground Blast Apparatus was used for schlieren studies which included an investigation of the effect of initial flow over the airfoil on the movement of the vortex. The results (ref. 6) showed that the initial flow was necessary for accurate simulation of the full-scale test conditions.

The purpose of this report is to present the first blast loads data obtained with the Ground Blast Apparatus. These data are in the form of pressure distributions along one chord of the wing of an airplane model. They were obtained for a condition in which the model, immersed at zero angle of attack in Mach number 0.7 flow, was struck normal to the surface of the wing by a blast wave which initially changed the angle of attack to about 20°. Two runs were made for this condition to establish the reliability of the results. Although the Ground Blast Apparatus and its operation are described in detail in reference 7, a brief description is included in this report.

SYMBOLS

c	airfoil section chord
C_m	pitching-moment coefficient about quarter-chord station
C_n	normal-force coefficient
M	Mach number
p	local measured pressure along chord, lb/sq in.
p/q	load coefficient
q	stream dynamic pressure, lb/sq in.
α	angle of attack, deg

TEST PROCEDURE

The schematic view of the NASA Ground Blast Apparatus at the NASA Wallops Station shown in figure 1 illustrates the procedure used to simulate the condition of an airplane in level flight being struck by a blast wave originating either directly above or below the airplane. An airplane model with its wings in the vertical plane is shown immersed in the flow of air which was initiated when pressurized air inside the shock tunnel was released by rupturing a diaphragm near the end of the tunnel nearest the model. To the left an explosive charge has been detonated and a portion of the resulting hemispherical blast wave is seen approaching the model. The detonation of the explosive charge is timed so that the resulting blast wave strikes the model only after sufficient tunnel flow has passed over the model to establish the steady-flow pattern of streamlines. When the blast wave strikes the model, pressure distribution measurements are obtained from which the loading caused by the blast wave is determined. A photograph of a test in progress is shown as figure 2. The model and the tunnel can be seen silhouetted against the fireball of the explosion in the background. The instant depicted is shortly after the blast wave has passed over the model. Simulation of blasts from directions other than those depicted in figures 1 and 2 can be obtained by rotating the model in roll in its sting support and/or by changing the location of the explosive charge.

APPARATUS AND INSTRUMENTS

Model

The model used in the present test is shown mounted on its sting support in figure 3. The geometric details of the model are shown in figure 4. It is a

midwing configuration identical to the wing-normal, basic configuration of reference 8. The wing has an NACA 65A006 airfoil section parallel to the plane of symmetry with the quarter-chord line swept back 45°, an aspect ratio of 4.0, and a taper ratio of 0.6. The wing, which is designed to be free of twist, incidence, or dihedral, is mounted symmetrically on a fuselage of circular cross section. The wing and the fuselage are made of steel.

The wing of the model (fig. 3) is instrumented to measure chordwise pressure distribution at the midsemispan. Flush diaphragm pressure transducers are mounted in both surfaces of the wing at 13 matching stations along the chord. Since only 12 recording channels are available, the 26 transducers provide a selection of measuring points to suit the test conditions and also provide alternate measurement points in case of pretest failure of a transducer. Four stations were chosen to define the pressure distribution on the surface toward the blast or "blast side." In both tests, these were the 5-, 22.5-, 52.5-, and 92.5-percent-chord stations. For the remaining eight on the surface away from the blast or "lee side," the seven at 5, 7.5, 15, 22.5, 32.5, 42.5, and 92.5 percent of the chord were chosen for both tests. The 75-percent-chord station was also chosen and used in test 1 but subsequent damage to the transducer made it necessary to shift to the 86-percent-chord station for test 2. The model also has a probe extending from the nose of the fuselage (fig. 3) to measure the total and static pressures of the airstream prior to the arrival of the blast wave.

Instrumentation

Pressure transducers and a companion 120-kilocycle carrier-amplifier system were developed at the Langley Research Center especially for measurements of transient pressures encountered in shock-tube and explosive work. A description of the system and its capabilities is presented in reference 9. The transducers are of the flush-diaphragm inductance type with an outside diameter of 0.187 inch and a thickness of 0.100 inch. The transducers have a pressure range of -15 to 30 lb/sq in. gage with ±1 percent linearity of full scale. The output due to acceleration is approximately 0.2 percent of full scale per 100g.

The pressure transducers are used in individual symmetrical bridge circuits. Since the transducers have only one coil, a "dummy" coil having the same inductance and resistance characteristics is required for the second leg of the bridge while the remaining two legs are matched resistors of a suitable value. To keep the pressure transducers and the remainder of the bridges in the same temperature environment, the dummy coils and resistors are located in the nose of the model. The air cavities inside the pressure transducers are connected by approximately 4 feet of fine tubing to manifolds that are also in the nose of the model. To avoid interactions between the transducers attached to the manifolds, the volume of the manifolds was made essentially infinite compared to the volume displaced by the deflection of the diaphragms of the transducers. By applying steady pressure or vacuum to the manifolds, however, a number of transducers may be calibrated simultaneously.

The output signal of the pressure transducers is fed into the 120-kilocycle carrier amplifier system which, in turn, directs the signal to dual-beam oscilloscopes. The system has a linearity of approximately ±1.5 percent of full scale

and a response flat up to 20 kilocycles. A low-pass filter cuts out frequencies above about 22 kilocycles. The oscilloscope traces are recorded photographically by an NASA 70-mm strip camera operating at approximately 20 feet per second. The traces are synchronized by recording a common pulse and thousand-cycle timing on each photographic film.

Blast gages located as shown in figures 1 and 3 were used to measure the side-on overpressure created by the blast. Pressure transducers of the type used in the model wing were mounted in a brass disk of $\frac{1}{4}$-inch maximum thickness and $2\frac{3}{4}$-inch diameter. The disks were oriented edge-on with respect to the direction of travel of the blast wave. The bridge was completed at the opposite end of the $1\frac{1}{4}$-inch-diameter tubing which supported the blast gage and the output was recorded in the same manner as the wing gages.

The total and static pressures of the airstream prior to blast-wave arrival were measured by small, commercial, strain-gage pressure transducers located in the nose of the model and connected by tubing to the orifices in the pressure probe. The transducers were used in a 3-kilocycle carrier amplifier system and the measurements recorded on an oscillograph. The overall response of this system was flat to approximately 300 cps.

A programer having 1-second steps was used to control various operations during the tests such as operating cameras and recorders and arming firing circuits. The programer also started an auxiliary millisecond time-delay system used to coordinate the blast-wave arrival with the operation of the shock tunnel.

Shock Tunnel

Details and operation.- The shock tunnel of the Ground Blast Apparatus is essentially a blowdown tunnel with the more conventional quick-opening valve replaced by a thin metal diaphragm. A detailed description of the tunnel and its operation is presented in reference 7. The tunnel is 10 feet in diameter and has a pressurized section 80 feet long. A 5-foot extension is provided downstream of the diaphragm to prevent the diaphragm segments from bending too far and tearing off after diaphragm rupture.

Because of the large size of the shock tunnel, the diaphragms were fabricated by butt-welding five pieces of sheet metal in the pattern shown in figure 5. The most satisfactory metal found for the present tests was cold-rolled annealed steel sheet in the range of SAE 1010 to SAE 1015 steel. This sheet was of 16 gage or approximately 1/16 inch thick. Also shown in figure 5 is the primacord used to rupture the diaphragm. It is arranged in the pattern shown and placed on the inside or pressure side of the diaphragm. When it is detonated, it cuts the diaphragm in eight pie-shaped segments and, being on the inside, speeds up the opening process. The eight-segment pattern was found to be an additional requirement that was necessary to prevent the segments from tearing off and going downstream with the airflow.

In operating the shock tunnel, it is desired that the airflow over the model have the same density and temperature as the surrounding still air in order that the blast wave, which originates outside the airstream, experience a minimum of interference in its travel toward the model. In order to accomplish this objective, the pressurized air inside the tunnel is heated by electrical strip heaters installed along the bottom of the tunnel. The temperature of the pressurized air is increased by an amount equal to the temperature drop which occurs when the pressurized air is released by the rupture of the diaphragm and expands isentropically to atmospheric pressure. Since the shock tunnel is constant in diameter along its length, the maximum Mach number obtainable is approximately 1. The constant-velocity portion of the flow from the tunnel has a duration of 50 to 70 milliseconds at $M = 0.7$. The tunnel pressure and temperature to achieve the desired conditions at a given Mach number were determined from standard shock-tube equations by the method outlined in appendix A of reference 6.

Flow characteristics.- As part of the development of the shock tunnel into an operational facility, the characteristics of the flow issuing from the tunnel were examined. A survey rake, composed of a number of total- and static-pressure probes extending from the leading edge of an airfoil-shaped strut, was placed 15 feet from the tunnel exit at the planned location of the model. Surveys were made with the rake spanning the jet at the three different positions indicated in figure 6. Also indicated in the same figure are the positions of the individual probes. Typical time histories of total and static pressures obtained during a survey are shown in figure 7. The sequence of events in the operation of this shock tunnel has been indicated by dividing the histories into five major regions. The first region, diaphragm rupture and primacord explosion, shows the pressure history at the rake of the spherically expanding shock or blast wave formed at diaphragm rupture by the sudden release of the tunnel pressure combined with the pressure caused by the explosion of the primacord. Following this, in the region labeled "flow development," the initial disturbances caused during diaphragm rupture are damped out and the flow steadies down to the condition shown by the relatively even pressure levels indicated by the total- and static-pressure measurements in the region labeled "steady flow." In order to insure that the steady-flow pattern of streamlines has been established over the model, the blast wave would be timed to strike the model during the end of the steady-flow period in the part of that period labeled "test time." The steady-flow period and test time are terminated when the portion of the blast wave from the primacord explosion which initially traveled into the shock tunnel appears at the measuring station after having been reflected from the inner end of the tunnel. As indicated earlier, the steady-flow period may vary from 50 to 70 milliseconds. The variation depends on the period required for the flow development which, in turn, depends upon how smoothly and rapidly the diaphragm opens after it is ruptured. The time period between the initial pressure pulse from diaphragm rupture to the appearance of the reflected primacord blast wave is essentially fixed by the length of the tunnel.

To illustrate the quality of the steady-flow period, the results of the survey taken on the vertical center line of the jet are presented in figure 8. They are typical of the results obtained at all three rake positions. Shown are envelopes of the flow variation during succeeding 10-millisecond intervals over the 50-millisecond period of steady flow just prior to the primacord blast-wave reflection, the period between 60 and 110 milliseconds in figure 7. It is apparent

that each succeeding envelope shows improvement in flow characteristics over the preceding envelope. The last two envelopes which include the test time indicated in figure 7 show that the steady-flow portion of the jet is about 8 feet in diameter. Although there were no measurements taken beyond those shown, it is estimated that the mixing region surrounding the main jet at this location was about 2 feet thick.

Explosive Charge

The explosive charges used for the tests were made of approximately 650 pounds of the aluminized explosive mixture HBX-1 cast in a hemispherical shape. Space in the base of the charge was provided for a 2-pound pentolite booster charge which, in turn, was provided with holes to receive the two instantaneous electric blasting caps used to initiate the detonation.

Rather than change the charge size to obtain different blast wave strengths at the model, the charge size is held constant and the distance between the charge and the model is adjusted to obtain the desired conditions. In the present case, the charge was located 125 feet from the model on a line perpendicular to the direction of the airflow from the tunnel. The firing position for the charge was at the top of a wooden tower approximately 12 feet from the ground. This height was chosen as a practical compromise between the desire to minimize loss of ground-reflected blast energy to cratering and the desire to keep the charge-handling problems within reasonable limits. It is estimated from reference 10 that between 80 and 90 percent of the blast energy striking the ground is reflected and that by the time the blast wave has reached a 40-foot radius, the reflected wave has combined with the initial blast wave to form a single wave called a Mach stem which is at least 10 feet high. By the time the blast wave has reached a radius of 72 feet, the limit of applicability of the data of reference 10, the Mach stem has reached a height of approximately 44 feet.

TESTS

Test Configuration

The first tests undertaken at the Ground Blast Apparatus measured chordwise pressure distribution at the midsemispan under conditions which simulated an airplane in level flight at $M = 0.7$ being struck by a blast wave originating from below in a direction normal to the flight path. The blast wave induced a particle or gust velocity at the model which caused an initial angle-of-attack change to a value about twice the steady-flow stall angle of the wing of the model. Two tests were conducted in order that the consistency of the data could be assessed.

In order to accomplish the simulation, the model was oriented on its sting mount with the wing in the vertical plane as shown in figure 2. To avoid the reflections of the blast wave from the tunnel during the test period, the model was positioned about 15 feet from the exit of the tunnel. Since the airstream is displaced by the blast wave, the model was placed about 18 inches from the center of the airstream in the direction of blast-wave passage to insure that the

model remained in the airstream during the test. A more complete discussion of the factors affecting the location of the model is presented in reference 7.

Blast-Wave Measurements

As stated previously, the actual blast-wave conditions were measured by a blast gage in the airflow near the model. In addition, the blast wave was measured at a point outside the airflow at a distance from the charge equal to that between the charge and the model. The two blast gages were oriented to measure the side-on overpressure in the blast wave. Measurements of the initial value of the time history of normally reflected or face-on overpressure in the blast wave were obtained from the pressure gage at 52.5 percent of the chord on the side of the wing facing the blast. For the first instant the wing gage measures the true face-on overpressures on an infinite plate but very shortly, pressure decay signals from the leading and trailing edges of the airfoil destroy these ideal conditions. The time histories of the side-on overpressure for the two tests are given by the solid lines in figure 9, and the time histories of wing pressure from which the initial values of the face-on overpressure were derived are given by the solid lines in figure 10. The curves in figure 9(d) are terminated at $5\frac{1}{2}$ milliseconds because of instrument malfunction. The remainder of the histories in figure 9 end at 10 milliseconds when the primacord blast-wave reflection terminates the test. Note that in figure 10 pressure is positive downward in conformity with the usual convention for airfoil pressures.

The dashed lines in figures 9 and 10 represent the faired time histories of pressure used in subsequent analysis. It is obvious that the fairing in some portions of the time histories is rather drastic. The justifications for the fairing procedure are presented in the discussions in the subsequent paragraphs.

Examination of the time histories of pressure in figures 9 and 10 shows that the start of each is characterized by a quickly damped transient oscillation. This oscillation is believed to represent the dynamic response of the measuring system to the almost instantaneous application of the blast-wave overpressure, and that the true value of pressure is a mean of the oscillations as represented by the faired curve. It is realized that the initial fairing of the pressures measured by the wing gage (fig. 10) is not theoretically correct since the decay in pressure until the signals from the finite edges of the wing reach the gage would be less than that indicated. However, since the period of time involved occurs during the initial transient oscillation, the true decay rate would be difficult to determine. As a result, the fairing shown was adopted since it would result in conservative loadings in subsequent analysis.

Comparison of the free air and tunnel flow measurements of the initial value of side-on overpressure for each test (fig. 9) shows immediately that the strength of the blast wave in the tunnel flow is considerably reduced. In addition, a second pressure peak appears on both the side-on and face-on pressure time histories in the tunnel flow (figs. 9 and 10) shortly after the beginning of the histories. Both the reduction in blast-wave strength and the second pressure peaks are attributed to reflections in the mixing zone surrounding the steady tunnel flow

through which the blast wave, which originates outside the tunnel flow, must pass to reach the model.

Experimental evidence that the mixing zone is the cause of the second pressure peak can be seen in the increase in the time of arrival of the second pressure peak at the blast gage (fig. 9) as compared with that at the wing (fig. 10). It is known that the thickness of a mixing zone surrounding a free jet increases with distance from its exit. Thus, at the blast gage, which is about 2 feet farther from the tunnel exit than the wing gage, the reflection which causes the second pressure peak must travel farther to reach that gage. Additional evidence of the increase in arrival time of the second pressure peak with distance from the tunnel exit was obtained in other tests where several blast gages were placed in the airstream at increasing distances from the tunnel exit. The possibility that the second pressure peak could be caused by reflections from the nearby fuselage appears to be refuted by these additional tests. The blast gages were mounted in such a manner that they were free of reflections from objects within the airstream and the second pressure peak still occurred.

The second pressure peak obviously represents a discrepancy in the simulation of the full-scale conditions but the energy in this peak is small compared with that in the main blast wave. It is believed that the simple course of fairing the second pressure peak out of any time history in which it appears adequately corrects for the discrepancy in simulation.

When the time histories of overpressure subsequent to the time of the second pressure peak are compared, it is evident that the overpressure time histories measured by the blast gage in the tunnel flow (figs. 9(b) and 9(d)) contain a relatively long-period oscillation which is not present in the other histories (figs. 9(a), 9(c), and 10). The blast gage in the tunnel flow is aft of the model and it is believed that the oscillations represent the radical change in the wake characteristics caused by the blast wave striking the model. Since the blast pressure histories measured at the wing (fig. 10) do not contain the oscillation, it is believed that the faired curves of figures 9(b) and 9(d) represent the side-on overpressure histories of the blast wave imposed on the wing.

Test Conditions

The initial conditions at blast-wave arrival for the two tests were as follows:

	Test 1	Test 2
Airstream velocity, V, ft/sec	794	785
Airstream Mach number, M	0.703	0.714
Initial blast-wave overpressure, lb/sq in.	5.78	5.58
Initial induced gust velocity, ft/sec	271	257
Angle-of-attack change, $\Delta\alpha$, deg	18.9	18.15
Atmospheric temperature, ^{o}F	67	41
Atmospheric pressure, lb/sq in.	14.87	14.79
Dynamic pressure, q, lb/sq in.	7.31	7.35
Distance from model to blast, ft	125	125
Duration of positive phase of blast (free air), msec	18	19

The initial values of induced gust velocity were calculated from the side-on blast-wave overpressure using the well-known Rankine-Hugoniot shock-wave relations. The angle-of-attack change was calculated as the change in direction of the relative wind vector obtained from the vector addition of the airstream velocity and the induced gust velocity. The initial dynamic pressure was then in turn calculated by using the velocity of the relative wind and taking into account the increased density of the airstream caused by the overpressure.

The Rankine-Hugoniot shock-wave relations can also be used to obtain a good approximation of the induced gust velocity subsequent to the initial shock. The time histories of angle of attack calculated by using gust velocity values computed from these relations are presented in figure 11.

RESULTS AND DISCUSSION

Time Histories of Pressures on Wing Chord

In order to provide an overall view of the pressure changes on the airfoil chord caused by the blast wave, the time histories of pressure change at each active gage for tests 1 and 2 are plotted in figures 12(a) and 12(b) at their position of measurement along the chord of the airfoil. The initial directions of travel of the airflow and blast wave are indicated at the left of the figure and time zero is defined as the instant the blast wave strikes the side of the airfoil toward the blast (blast side). Note that the histories are plotted so that time increases with distance away from the airfoil; that is, on the blast side, time increases to the left and on the side away from the blast or lee side, time increases to the right. The pressure scale, which is common to all the histories, is shown at the lower left of each figure. The dashed curve plotted with each of the blast-side pressure histories is the faired history of the side-on overpressure of the blast wave measured aft of the model taken from figure 9(b).

Comparison of the time histories of pressure measured in tests 1 and 2 (figs. 12(a) and 12(b)) shows that they are very similar in magnitude and shape. The simpler histories on the blast side are nearly alike and those on the lee side where the flows are much more complicated differ only in fine detail. The comparison indicates, then, that, even though the initial angle-of-attack changes are to a value much greater than the steady-state stall angle of the airfoil where turbulent separated flows are normally expected, the major pressure changes follow the same sequence under the same initial conditions. The consistency of the data also indicates that the reliability of the test technique and the instrumentation system is established.

Other things can be learned about the processes of the blast loading of the airfoil by more detailed examination of the pressure time histories. The histories of pressure change at all the gages on the blast side of the airfoil begin with an almost instantaneous jump in pressure to a value about $2\frac{1}{2}$ times the initial side-on pressure measured by the blast gage (dashed line). This difference in pressure is representative of that measured by side-on and face-on blast gages in free air at this same overpressure level. It is apparent, however, that the

pressures subsequently reduce more quickly (ignoring the second pressure peak) at the trailing edge of the airfoil than at the leading edge. Since, without airflow, the pressures would be expected to reduce at an equal rate on the leading and trailing edge as the blast wave diffracts around the airfoil, it is apparent that the airflow tends to retain the pressure over the forward portion. As a result, the center of pressure on the blast side which initially is at the 50-percent-chord point shifts forward as time passes.

The progress of the diffraction of the blast wave over the lee side of the airfoil can be followed by observing the sequence of arrival of the first pressure signal at the gage locations. As might be expected, the airflow causes an unsymmetrical diffraction of the blast wave around the leading and trailing edges. The available time resolution on the individual records and in the synchronization between them, however, precludes an accurate determination of the progress of the diffraction based on measurements from the records. Because of this difficulty, a simple calculation was made to estimate the chordwise meeting point of the two portions of the diffracting wave. Taken into account in the calculation were the average local airstream velocities over the parts of the airfoil chord traversed by each portion of the wave and the estimated velocities that each portion of the diffracting wave would have in still air. The still air velocity of the wave diffracting from the leading edge was assumed to be a function of the average maximum positive pressure measured as the wave passed over the gages from 5 to 42.5 percent of the chord (fig. 12(a)) and, similarly, the still air velocity of the portion of the wave diffracting from the trailing edge was assumed to be a function of the pressure measured by the gages at the 92.5- and 75-percent-chord stations. The results of the calculation are shown as the time-distance plot (fig. 13) where the solid line shows the progress of diffraction from the leading edge and the dashed line the progress from the trailing edge. The circles on the figure represent the best measurements from the original records of the time of arrival of the diffracting wave at each gage on the wing chord. It is seen from the figure that the approximate calculation predicts the meeting point of the two portions of the diffracting wave to be the 78-percent-chord position at about 0.6 millisecond after the blast wave strikes the airfoil. The experimental data, if the obviously erroneous point at 32.5 percent chord is ignored, also indicate a meeting point of the waves in the 75- to 80-percent-chord region. In order for the diffraction to be completed in the time indicated by the experimental data, however, the wave diffracting from the leading edge would require an overpressure of approximately 20 lb/sq in. to obtain the necessary velocity while the actual measured overpressure (fig. 12(a)) was only about 2 lb/sq in. It is believed that the calculated pattern is a reasonably accurate representation of the diffraction process. The experimental data, although suffering from inadequate time resolution in this case, provide a qualitative check on the meeting point of the two portions of the diffracting wave.

In figure 12 it is noted that the initial pressure change measured by all the lee-side gages is in the positive direction but that the magnitude of the change is much less over the leading portion of the airfoil than from the 75-percent station aft. The positive pressure obviously represents the overpressure in the portions of the diffracting blast wave and, if there were no airflow, the magnitudes would be expected to be equal or at least symmetrical about the 50-percent-chord station.

Further examination of the histories of pressure change on the lee side of the airfoil (fig. 12) shows that the initial positive pressure is followed by an abrupt change to high negative pressure. This negative pressure is attributed to a strong vortex formed at the leading edge during the diffraction process which is free to travel back along the chord. This premise is supported by tests made at low speed (ref. 3) and further by small-scale schlieren studies representing the present test condition (ref. 6). In the time histories of figure 12(a), the position of the vortex along the chord at a particular time can be seen clearly as far back as the 42.5-percent-chord station by observing the time at which the maximum negative pressure reaches each measuring station. This criterion does not appear to apply at the 75- and 92.5-percent-chord stations since the effect of the vortex on the pressures at these stations is believed to be obscured by the pressures in the wave diffracting around the trailing edge and those in the associated separated flow. When only the times of arrival of the vortex up to the 42.5-percent-chord station are used, the estimation is made that it requires about 5 milliseconds or about 3 chords of flow for the vortex to move from the leading to the trailing edge of the airfoil. This result is in agreement with the results of the low-speed tests of reference 3 and falls within the scatter of the results of the small-scale, high-subsonic speed, schlieren studies of reference 6.

Pressure Distributions on Wing Chord

The pressure distributions for test 1 are given in figures 14(a) through 14(y) for 0.1-millisecond intervals from 0 to 0.5 millisecond and for 0.5-millisecond intervals from 0.5 to 10 milliseconds after arrival of the blast wave at the wing. The pressure time histories of figure 12(a) were first faired in a manner similar to that indicated in figures 9 and 10 and the pressures for each time read from the faired histories. These individual pressures p were then divided by the value of dynamic pressure q acting at the corresponding time and the resultant values plotted against the gage position in percent chord. The solid lines faired through these points represent the pressure distribution on the airfoil. It should be noted that, since the pressure time histories of figure 12(a) are referenced to the pressures at the measuring stations prior to the arrival of the blast wave, the pressure distributions of figure 14 are similarly referenced to the ambient conditions prior to the blast. While the pressure distributions thus referenced represent the actual transient loading of both sides of the wing chord, such referencing results in unrealistic pressure distributions from the aerodynamic point of view. To present the distributions from the proper aerodynamic standpoint, the horizontal dashed lines were added to the pressure distributions to indicate the instantaneous ambient static pressure, which is generally the reference pressure used in plotting pressure distribution. The position of these lines was determined by dividing the instantaneous value of side-on overpressure in the blast wave by the corresponding value of the dynamic pressure. Included in the legend for each pressure distribution is the instantaneous value of angle of attack α taken from figure 11. No pressure distributions are presented for test 2 because of the lack of sufficient pressure data on the lee side of the airfoil.

The distributions in figures 14(a) to (f) illustrate the diffraction of the blast wave around the airfoil. At time zero, the blast wave has just struck the

blast side of the airfoil; at time 0.1 millisecond, it has diffracted around the leading and trailing edges and imposed pressure at the 5-, 7.5-, and 15-percent-chord stations on the lee side of the airfoil. The broken line beyond the 15-percent-chord station represents the estimated further progress of the wave diffracting from the leading edge and the broken line from the trailing edge similarly estimates the progress of the wave diffracting from that direction. The succeeding distributions show the further progress until at 0.5 millisecond all gages have received pressure signals.

The initial formation of the leading-edge vortex can also be seen in the series of pressure distributions covering the first 0.5 millisecond. The succeeding distributions at 0.5-millisecond intervals to 4.0 milliseconds show the travel of the vortex along the chord. The first evidence of the negative pressure, indicating the vortex, appears at 0.2 millisecond (fig. 14(c)) where the pressure at the 5-percent-chord station is seen to have dropped to zero from the positive value indicated at 0.1 millisecond. From 0.2 millisecond to 0.5 millisecond (figs. 14(c) to (f)), the negative pressure area at the leading edge increases in size and intensity. Figure 14(g), at 1.0 millisecond, shows that the negative pressure area has widened out, indicating that the vortex is breaking away from the leading edge and figure 14(h), at 1.5 milliseconds, to figure 14(m), at 4.0 milliseconds, show clearly the negative pressure peak associated with the movement of the vortex along the chord. Actually, due to the lack of measurements between the 42.5- and 75.0-percent-chord stations, the movement and shape of the pressure peak in that region represent an estimation (figs. 14(k) to 14(m)). Comparison of the traveling pressure peak found in these tests with that found in the tests of reference 1 shows that the present peak is much less pronounced. It is believed that this is a logical result inasmuch as the tests of reference 1 were for initial angle-of-attack changes nearly twice that of the present tests and it might be expected that the vortex would be stronger.

The remainder of the pressure distributions (figs. 14(n) to 14(y)) shows the after effects of the passage of the vortex together with the results of the efforts of the flow to accommodate itself to the rapidly decreasing angle of attack. It should be noted that, despite the rapidly changing shapes of the pressure distribution on the lee side of the airfoil, the distributions on the blast side are very regular in shape and decrease in an orderly manner after the initial pressure is imposed on the airfoil.

Loads and Moments on Wing Chord

Normal-force coefficients were obtained by integrating the pressure distributions of figure 14. The resultant values are shown in figure 15 (solid line) plotted against both time and airflow (measured in chords) over the airfoil section. Also plotted in the figure is a dashed line showing the contribution to the normal-force coefficient of the pressures imposed on the blast side of the airfoil alone. The difference between the solid and dashed lines represents the contribution of the pressures measured on the lee side of the airfoil. It is apparent from comparison of the two curves that, in the early portion of the time history, the loading is almost entirely produced on the blast side of the airfoil.

After about $2\frac{1}{2}$ milliseconds, however, the negative pressures generated on the lee side of the airfoil become an important part of the total loading imposed on the airfoil.

In order to provide a basis for estimating the importance of the blast loading, the normal-force coefficients are shown plotted against their corresponding instantaneous angle-of-attack values in figure 16. Also shown in the figure is a dashed curve showing the steady-flow variation of normal-force coefficient over the angle-of-attack range from 0° to 20°. The steady-flow curve was derived from data presented in reference 11 which describes the results of wind-tunnel tests on a model one-third the scale of the present model. Comparison of the two curves shows immediately that the loading caused by the blast is considerably higher than that obtained at the same angle of attack in steady wind-tunnel tests. The initial blast loading (at 18.8°) is more than twice the steady-flow value and, although the loading drops rapidly, it remains well above the maximum static normal-force coefficient until the blast-induced angle of attack drops to 10°.

In addition to determining the normal-force coefficients from the pressure distributions of figure 14, the pitching-moment coefficients about the quarter chord of the airfoil were also obtained. These coefficients are plotted against angle of attack and compared with those from the steady-flow wind-tunnel tests in figure 17. It is immediately apparent that the pitching-moment coefficients obtained in the blast-load tests are much greater than those obtained in the wind-tunnel tests. The initial value of -0.5 is the result of the almost rectangular pressure distribution along the side of the airfoil facing the blast. The rapid initial reduction in the value of C_m reflects the growth of the vortex at the leading edge. The subsequent increase of the value results from the movement of the vortex along the chord and the second decrease, more gradual than the first, is primarily caused as the pressures on the side of the airfoil facing the blast become lower at the trailing edge than at the leading edge. In the low-speed results of reference 1, the initial high negative values of pitching-moment coefficient were not obtained because the instrumentation did not have sufficiently high response characteristics. The subsequent trends, however, are identical to the present case. That the first points obtained in the low-speed tests are positive is due to the relatively stronger influence of the vortex in that case.

To further emphasize the dynamic structural problems caused by the extreme values and variations of the pitching moments obtained in blast loading, histories of the variation of the pitching-moment coefficient about the quarter chord and the corresponding variation of the center-of-pressure position are shown in figures 18(a) and 18(b), respectively, with both time and flow. It is apparent from examination of these figures that not only is a high torsion load imposed on the airfoil at the first instant by the nearly rectangular pressure distribution imposed on the blast side of the airfoil but that after a rapid decrease the loading again builds up when the traveling vortex moves along the chord. This loading sequence should probably be considered as a possible source of excitation of the torsional modes of a wing structure.

CONCLUDING REMARKS

An experimental investigation of blast loading on airfoils at flow speeds of Mach number 0.7 has shown that, for a blast wave which instantaneously changes the angle of attack on the airfoil from 0° to 18.8°, the resultant loading and values of pitching-moment coefficient are considerably greater than those obtained in steady-flow wind-tunnel tests. As in earlier low-speed investigations, a major factor in the higher loadings appears to be a vortex formed at the leading edge during the diffraction of the blast wave around the airfoil section which moves aft at about one-third the stream velocity. The excellent response characteristics of the instrumentation allowed the first direct detailed pressure measurements of the diffraction of a blast wave around an airfoil.

Langley Research Center,
National Aeronautics and Space Administration,
Langley Station, Hampton, Va., November 6, 1962.

REFERENCES

1. Pierce, Harold B., and Reisert, Thomas D.: Initial Experimental Investigation of the Aerodynamic Load on the Wing of a Model Caused by a Blast-Induced Gust That Increases the Angle of Attack Into the Stall Region. NACA RM L55H22b, 1955.

2. Pierce, Harold B., and Spahl, Raymond J.: Experimental Investigation To Determine the Loads on a Horizontal Tail of a Model Caused by a Blast-Induced Gust. NACA RM L57A28a, 1957.

3. Pierce, Harold B., and McFarland, Donald R.: Experimental Results on Wing Loads Due to Blasts. NACA RM L57D22a, 1957.

4. Ruetenik, J. Ray: Evaluation of Traveling-Gust Method for Airfoils in Strong Blast Waves by Shock-Tube Tests. WADD Tech. Rep. 60-279, U.S. Air Force, May 1960.

5. Ballard, R. L., Hoffman, A. J., and Baker, W. E.: An Experimental Investigation of the Effect of Motion of a B-29 Horizontal Stabilizer on External Blast Damage From Explosive Charges. Rep. No. 982, Ballistic Res. Labs., Aberdeen Proving Ground, June 1956.

6. McFarland, Donald R.: Investigation of Vortex Movements About a Wing in Intermediate and High Subsonic Flow Undergoing a Large Angle-of-Attack Change in a Blast-Induced Gust. NASA TN D-1238, 1962.

7. Pierce, Harold B. (With appendix by Richard W. Morton): Interaction of Blast Waves With Wings - Part I. Ten-Foot Diameter Free Jet Shock Tube. Proc. Third Shock Tube Symposium, SWR-TM-59-2, U.S. Air Force, Mar. 1959, pp. 271-291.

8. West, F. E., Jr., Liner, George, and Martz, Gladys S.: Effect of Leading-Edge Chord-Extensions on the Aerodynamic Characteristics of a 45° Swept-back Wing-Fuselage Combination at Mach Numbers of 0.40 to 1.03. NACA RM L53B02, 1953.

9. Morton, Richard W., and Patterson, John L.: A Transient Pressure Measurement System for Blast Effect Research. [Preprint] 148-LA-61-1, Instrument Soc. of America, Sept. 1961.

10. Bryant, E. J., Eberhard, R. A., and Kingery, C. N.: Mach Reflection Over Hard Packed Dirt and Dry Sand. Rep. No. 809, Ballistic Res. Labs., Aberdeen Proving Ground, July 1952.

11. Loving, Donald L., and Williams, Claude V.: Aerodynamic Loading Characteristics of a Wing-Fuselage Combination Having a Wing of 45° Sweepback Measured in the Langley 8-Foot Transonic Tunnel. NACA RM L52B27, 1952.

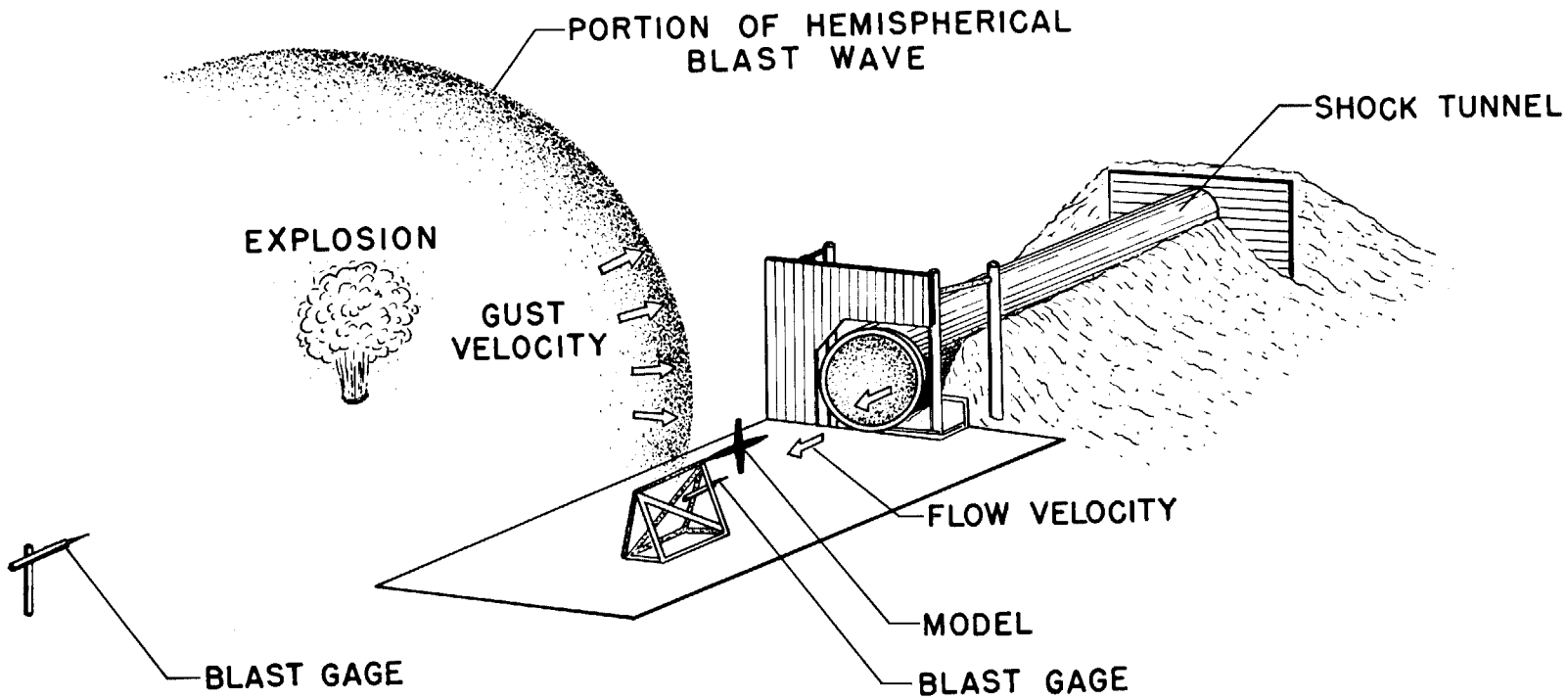

Figure 1.- Blast research with fixed model.

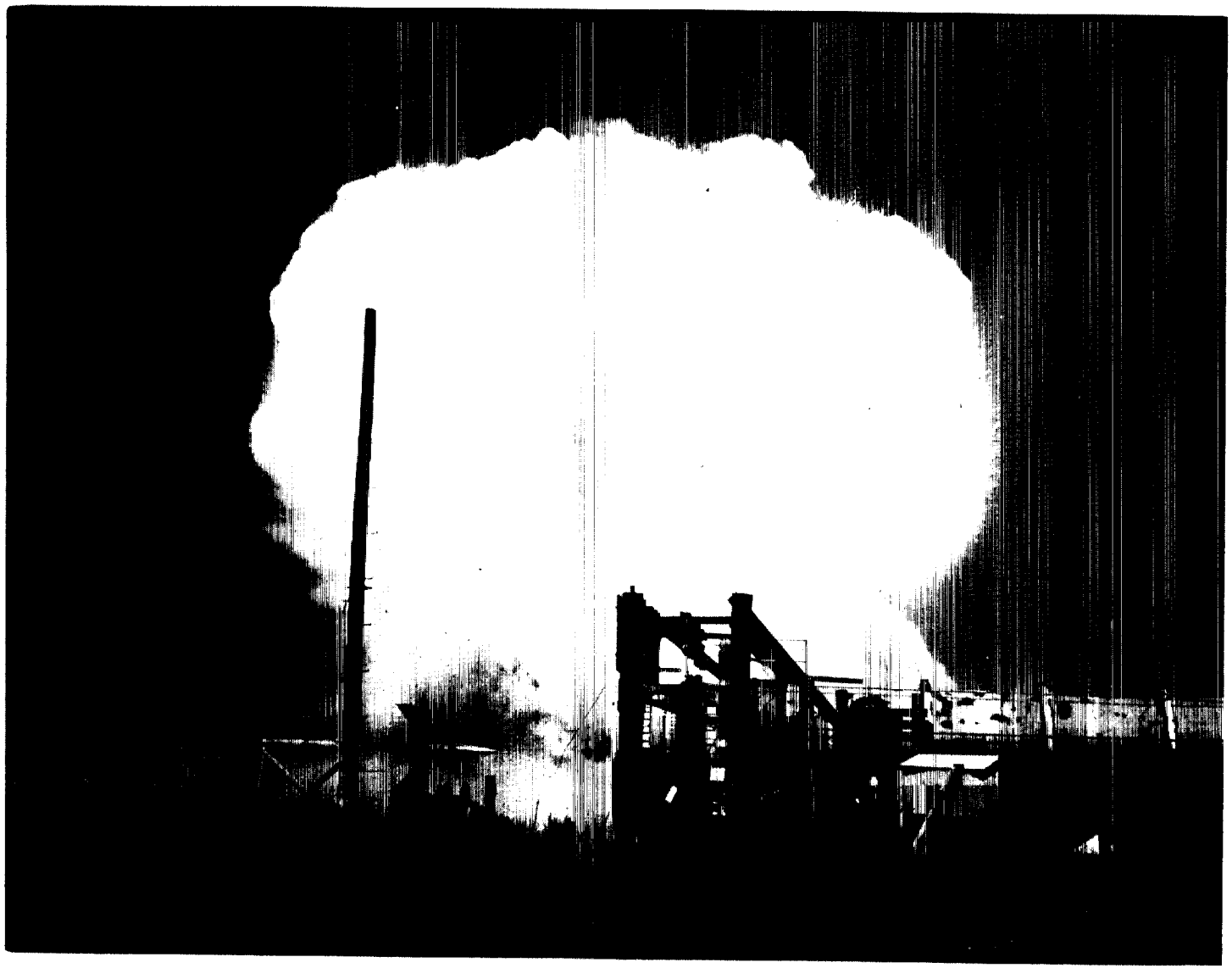

Figure 2.- Test in progress. L-60-5886

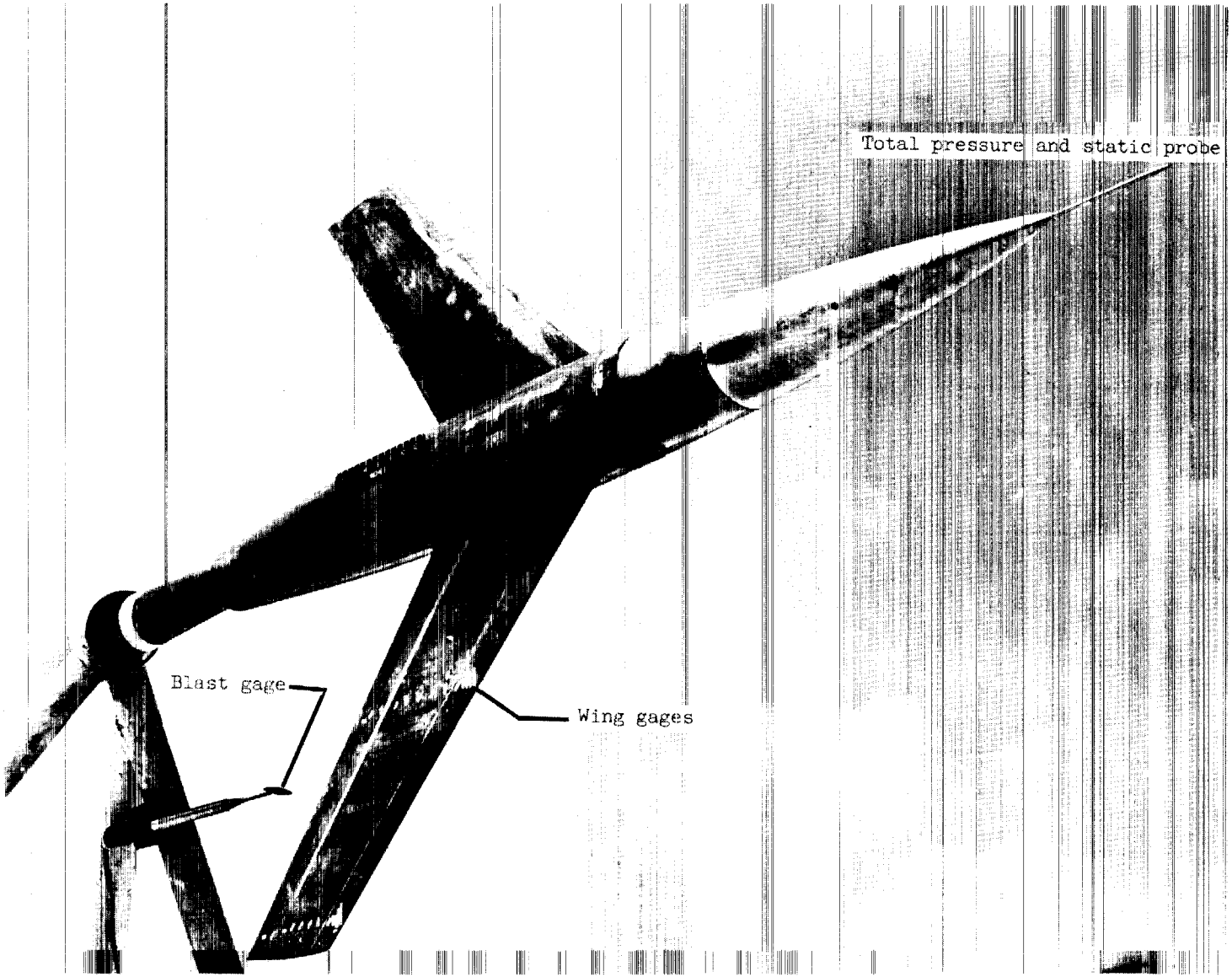

Figure 3.- Photograph of model. L-60-5852.1

Wing Details

Taper	0.6
Aspect ratio	4.0
Wing area, sq ft	9
Incidence, deg	0
Dihedral, deg	0
Geometric twist	0
Airfoil section	NACA 65A006 (parallel to plane of symmetry)

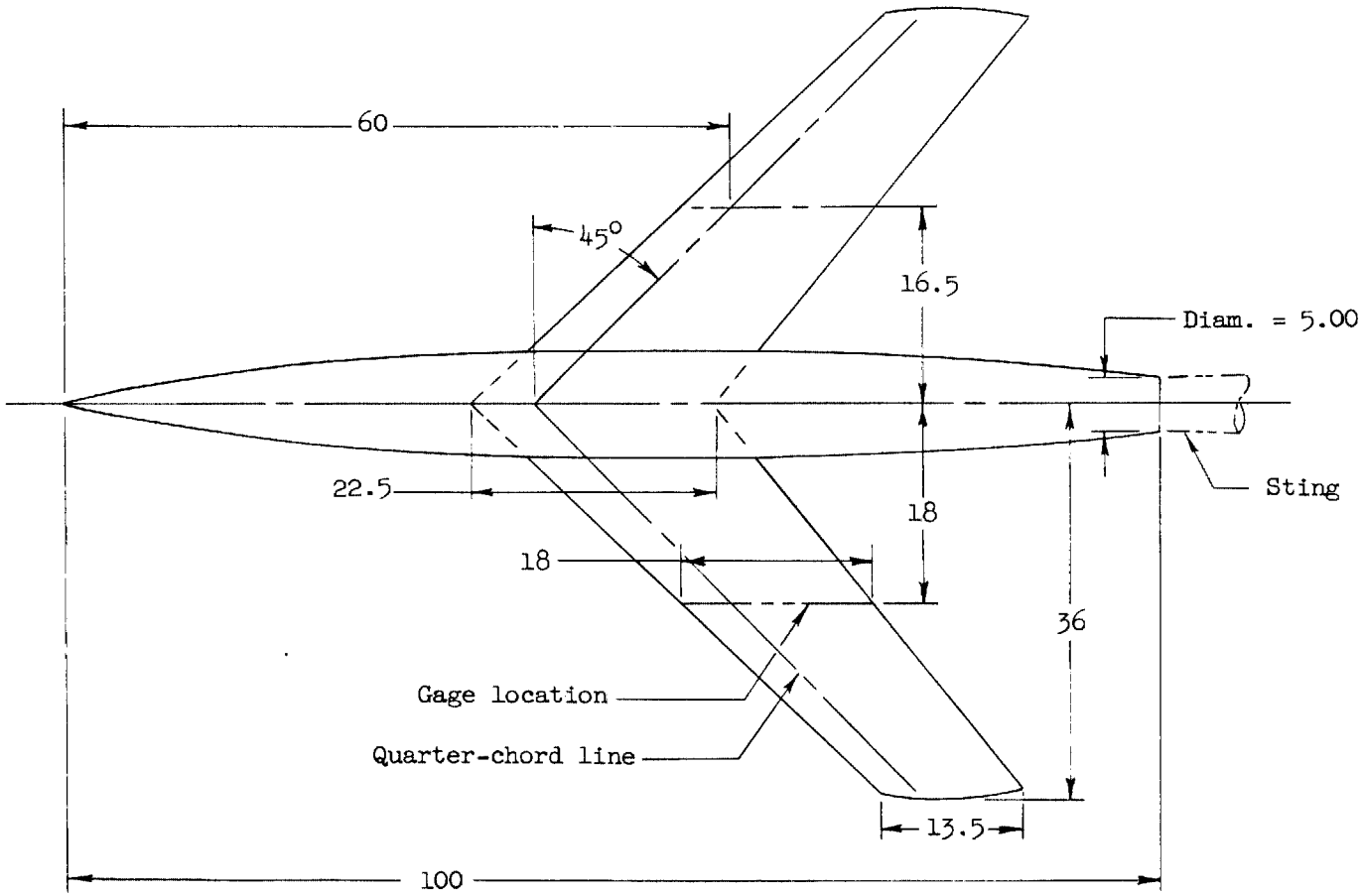

Figure 4.- Model details. All dimensions are in inches.

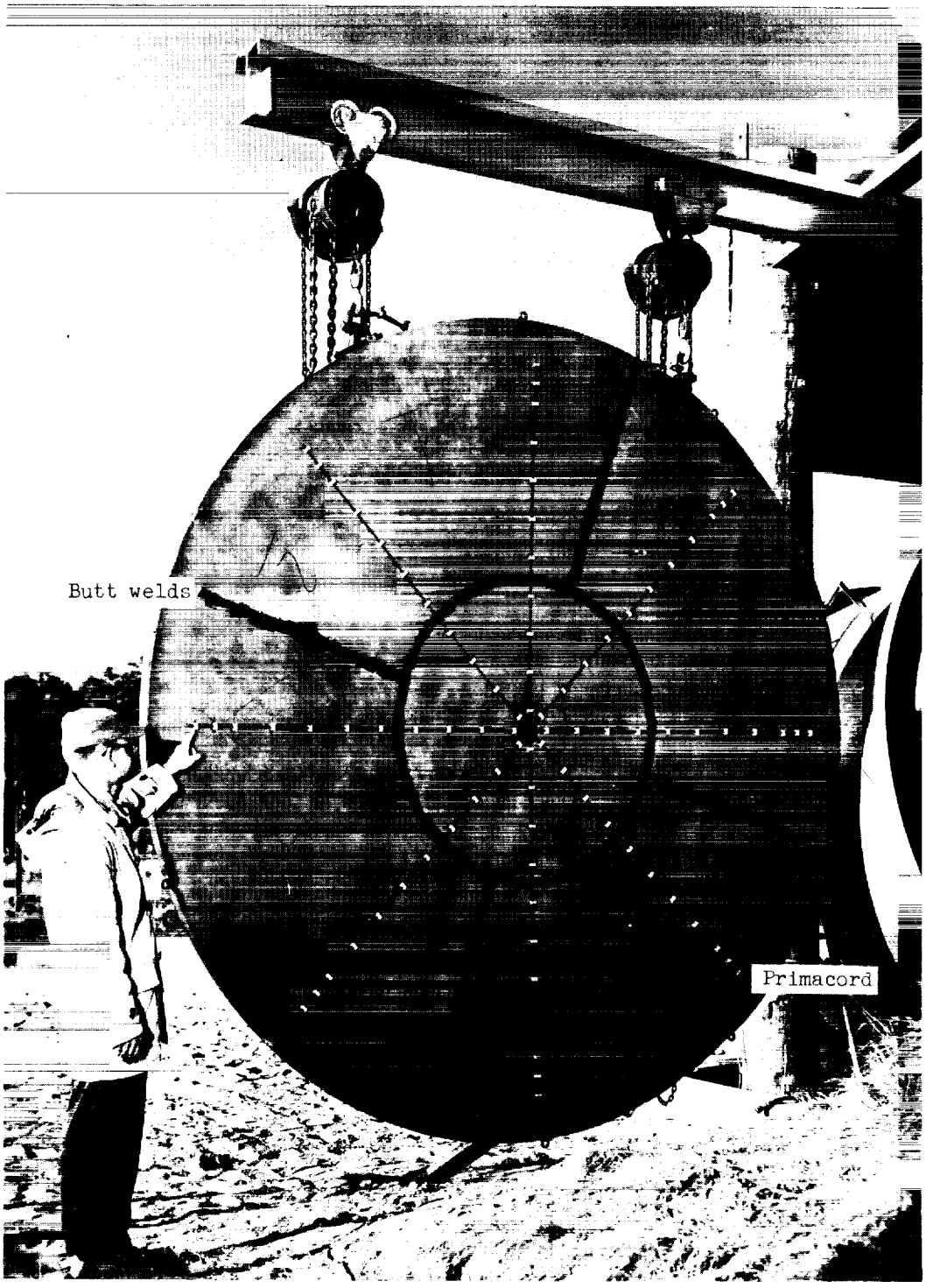

Figure 5.- Photograph of diaphragm. L-59-1318.1

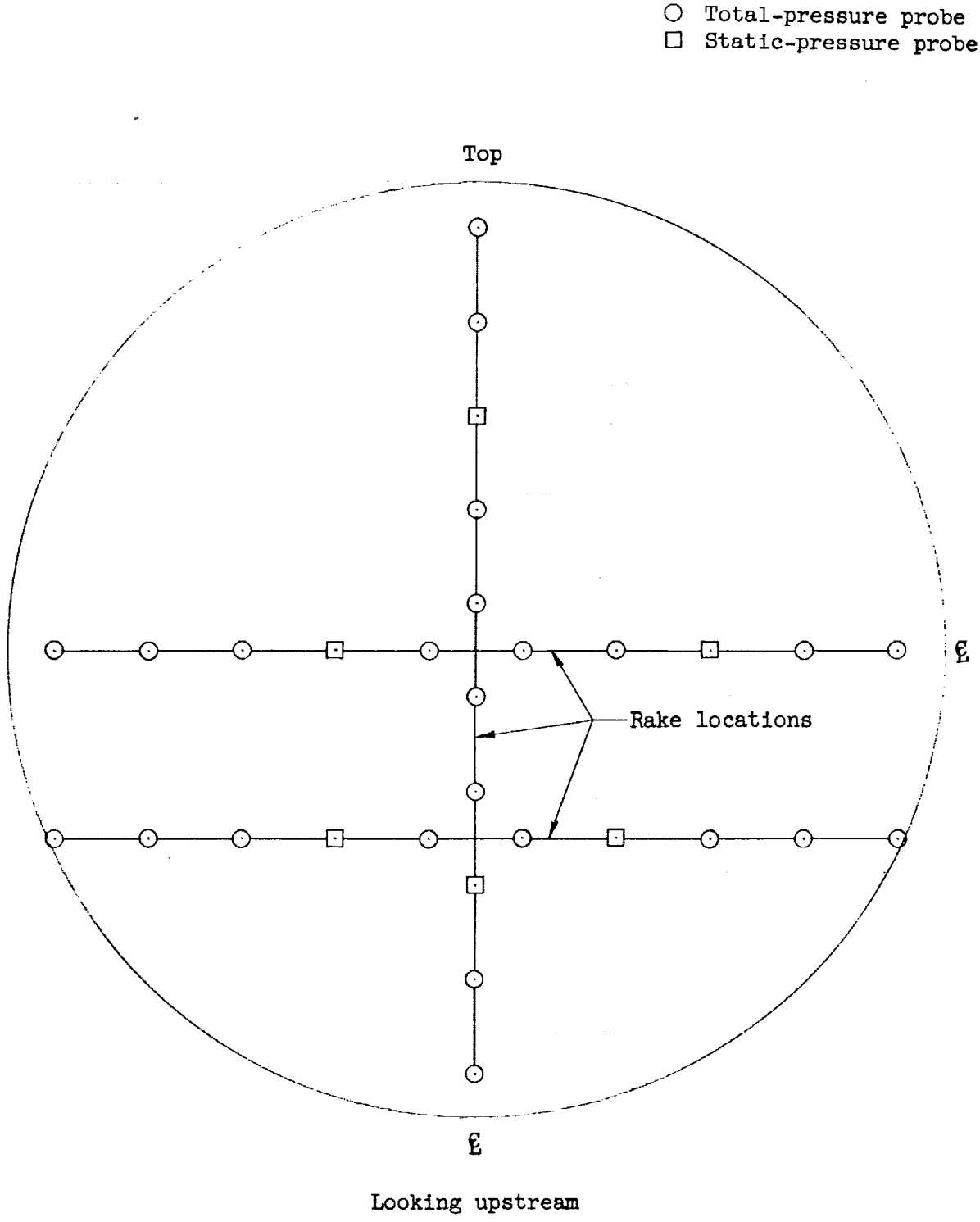

Figure 6.- Rake and gage locations for flow survey.

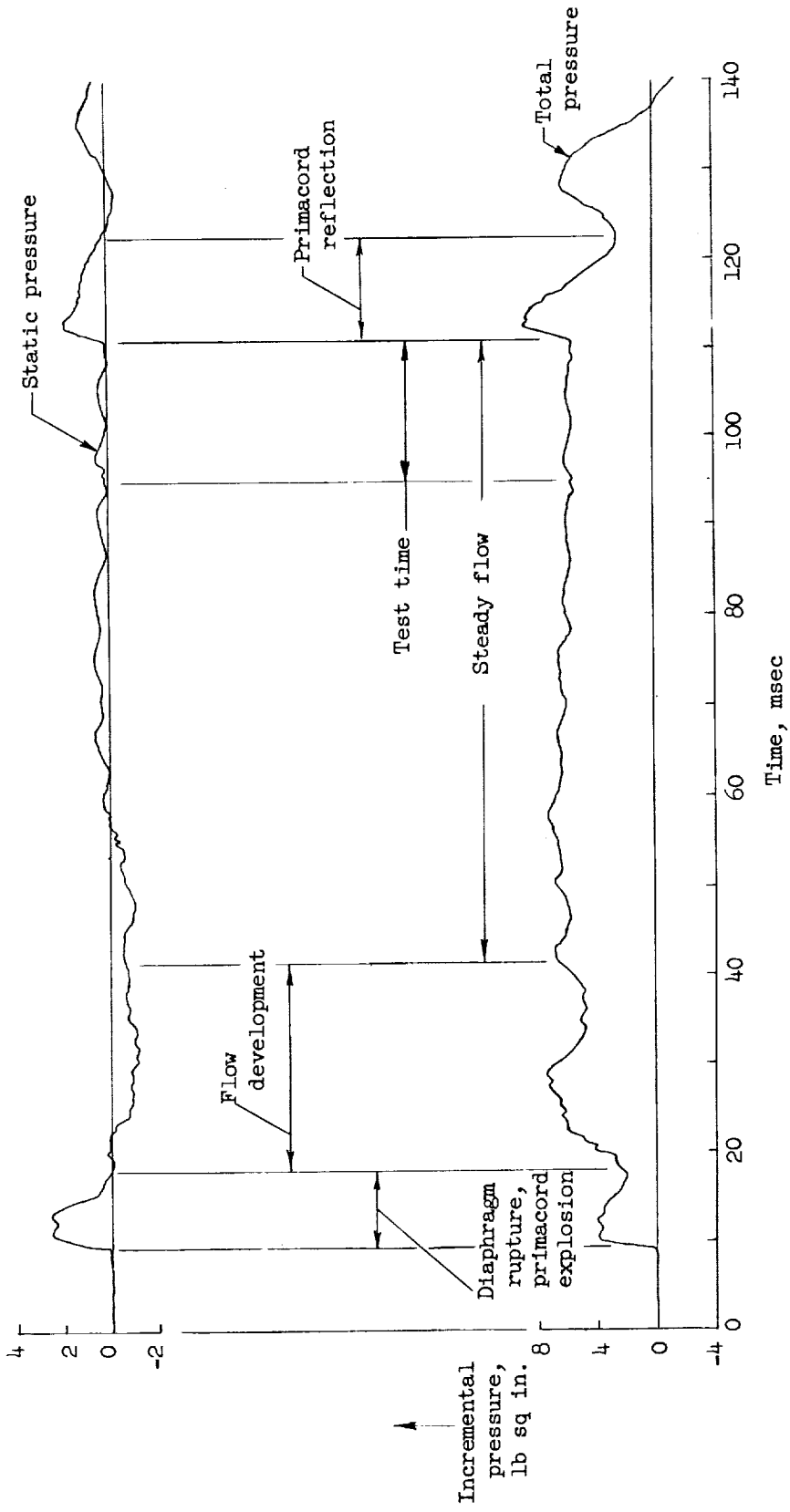

Figure 7.- Time history of flow events.

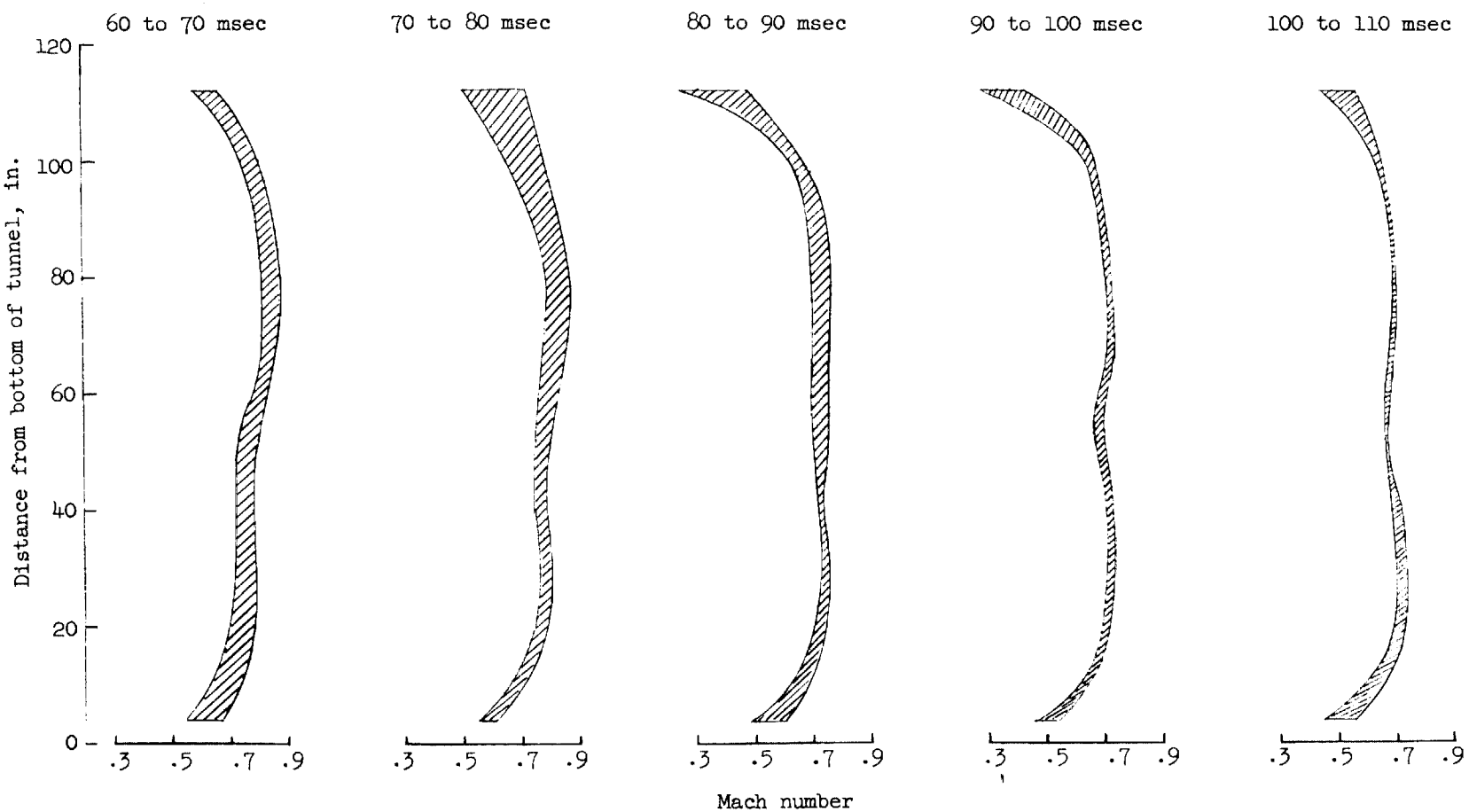

Figure 8.- Flow survey at model.

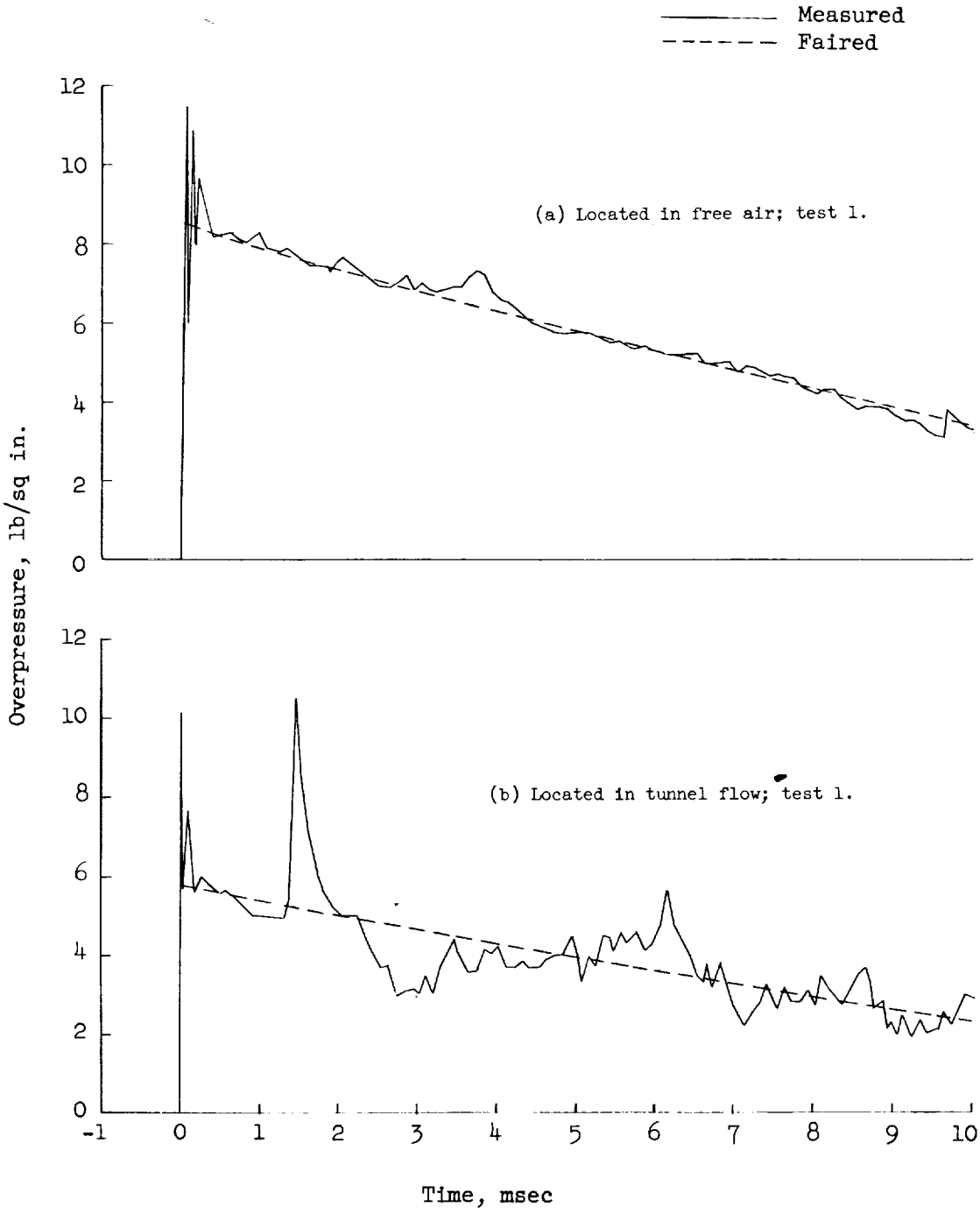

Figure 9.- Overpressure time histories of blast gages.

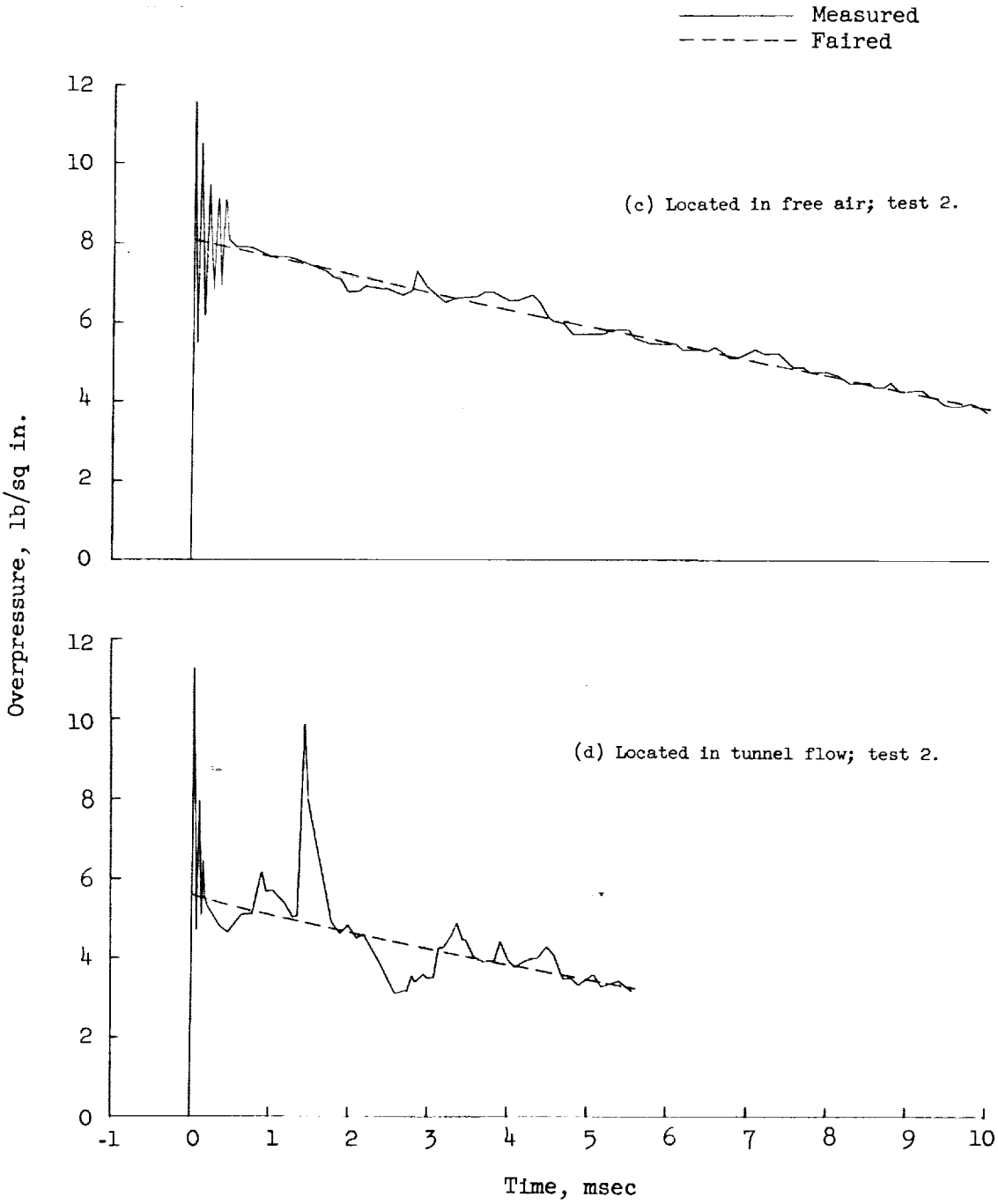

Figure 9.- Concluded.

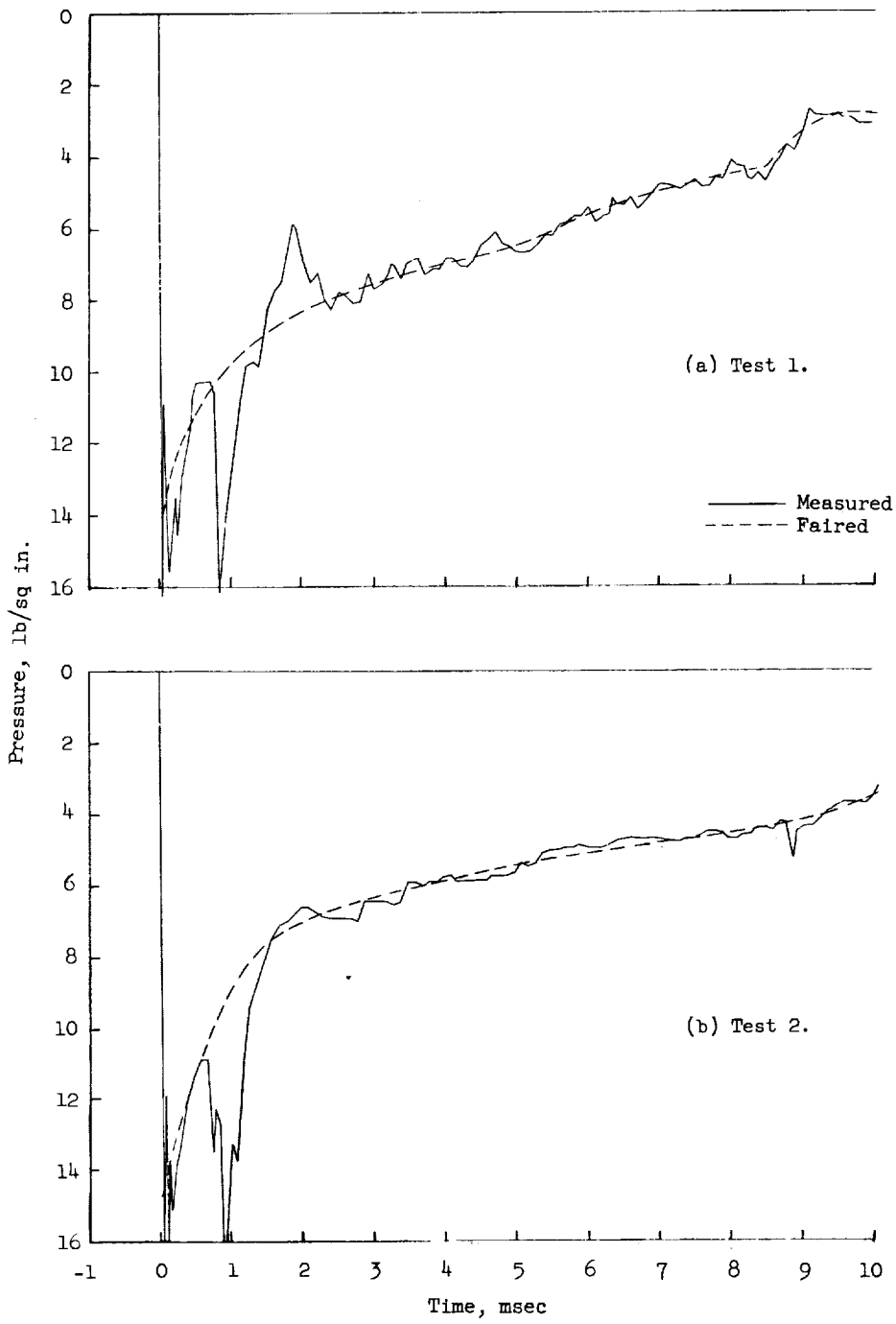

Figure 10.- Pressure time histories at blast-side 52.5-percent-chord station.

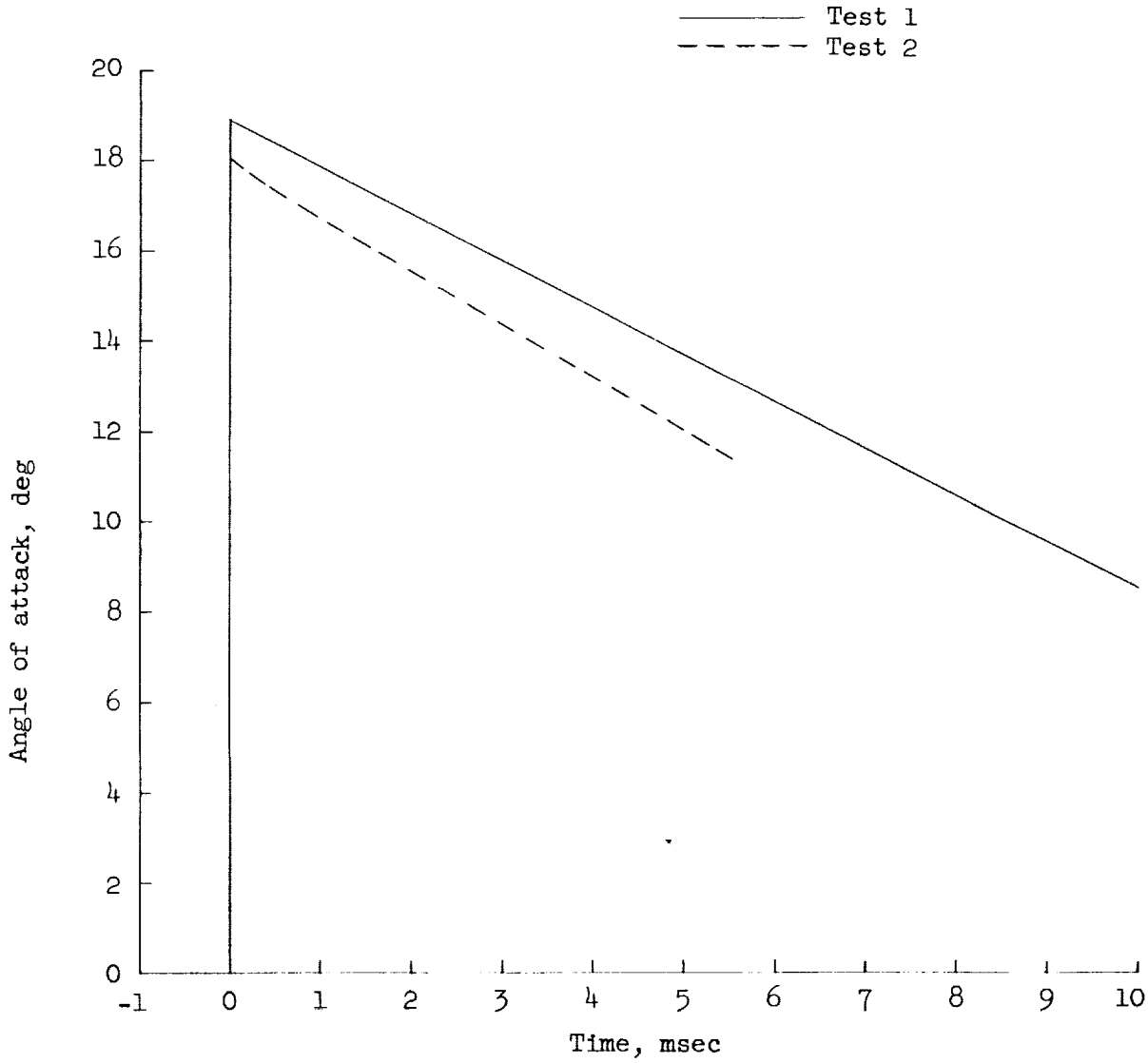

Figure 11.- Angle-of-attack variations.

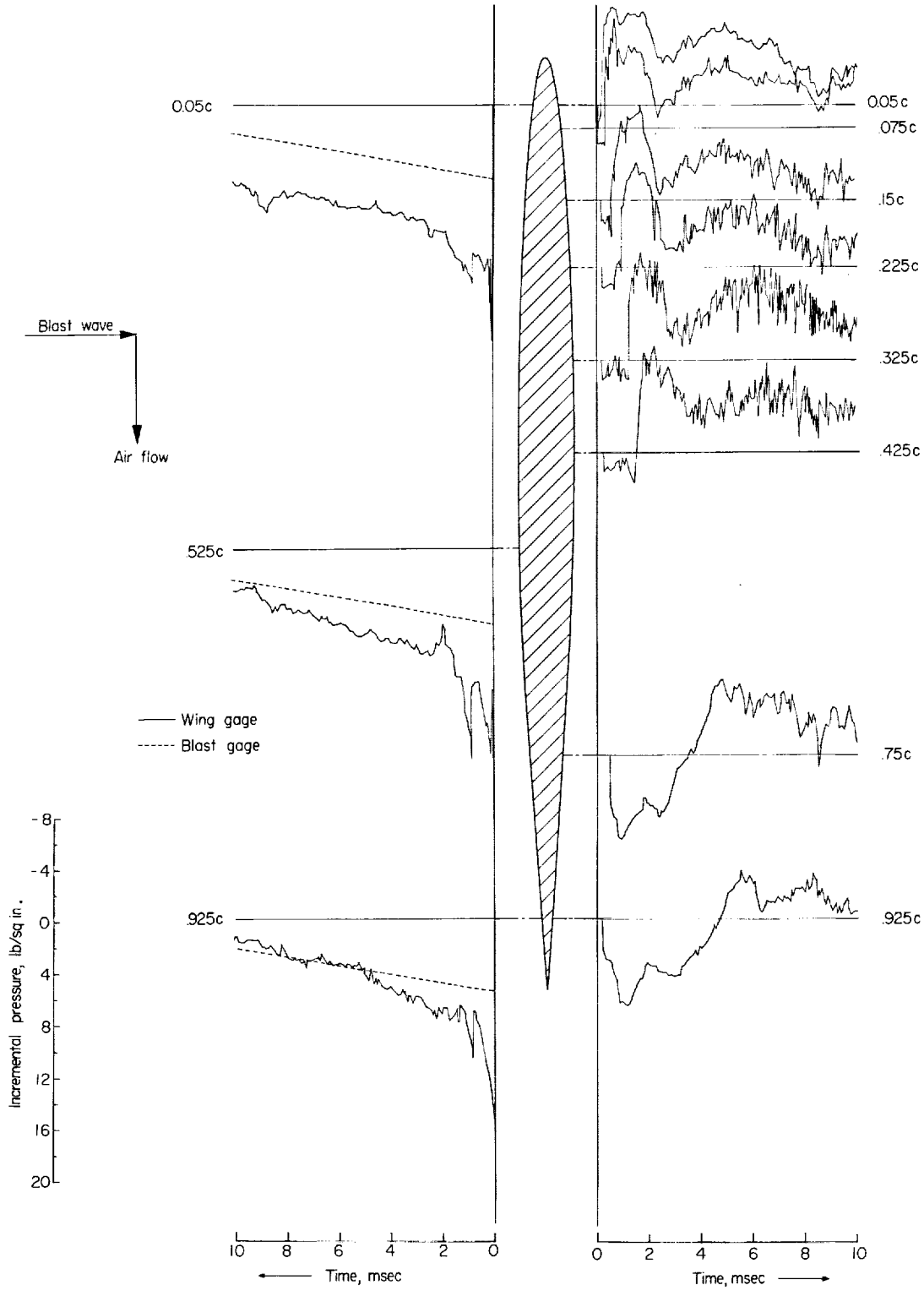

(a) Test 1.

Figure 12.- Pressure time histories on wing chord.

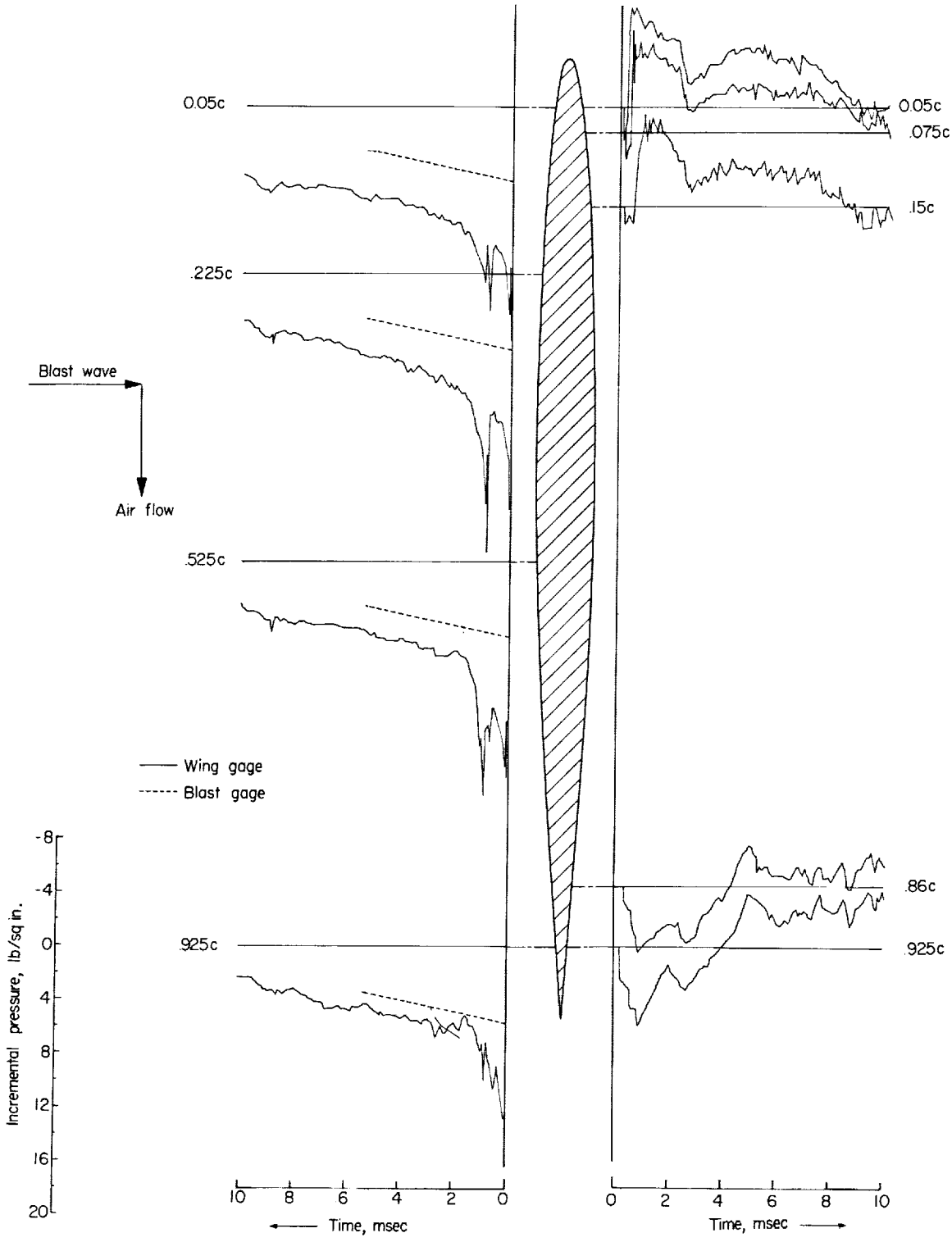

(b) Test 2.

Figure 12.- Concluded.

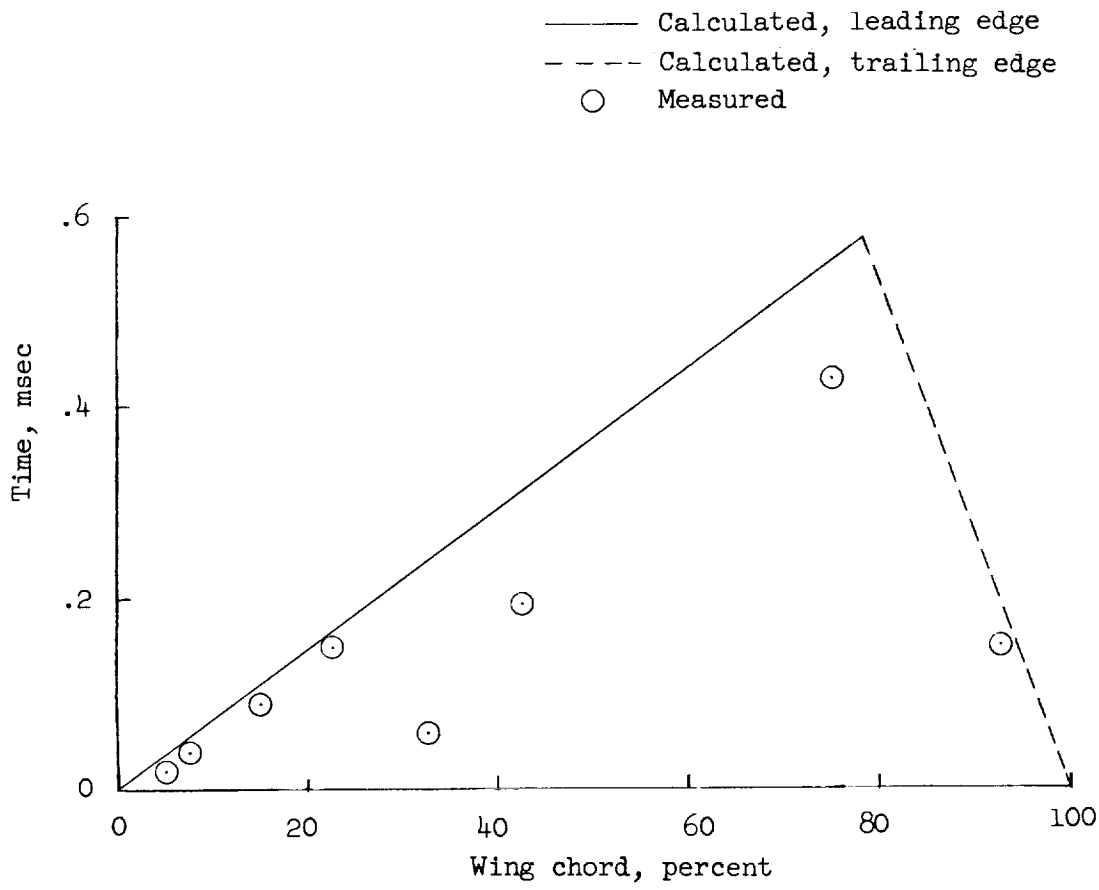

Figure 13.- Diffraction of blast wave.

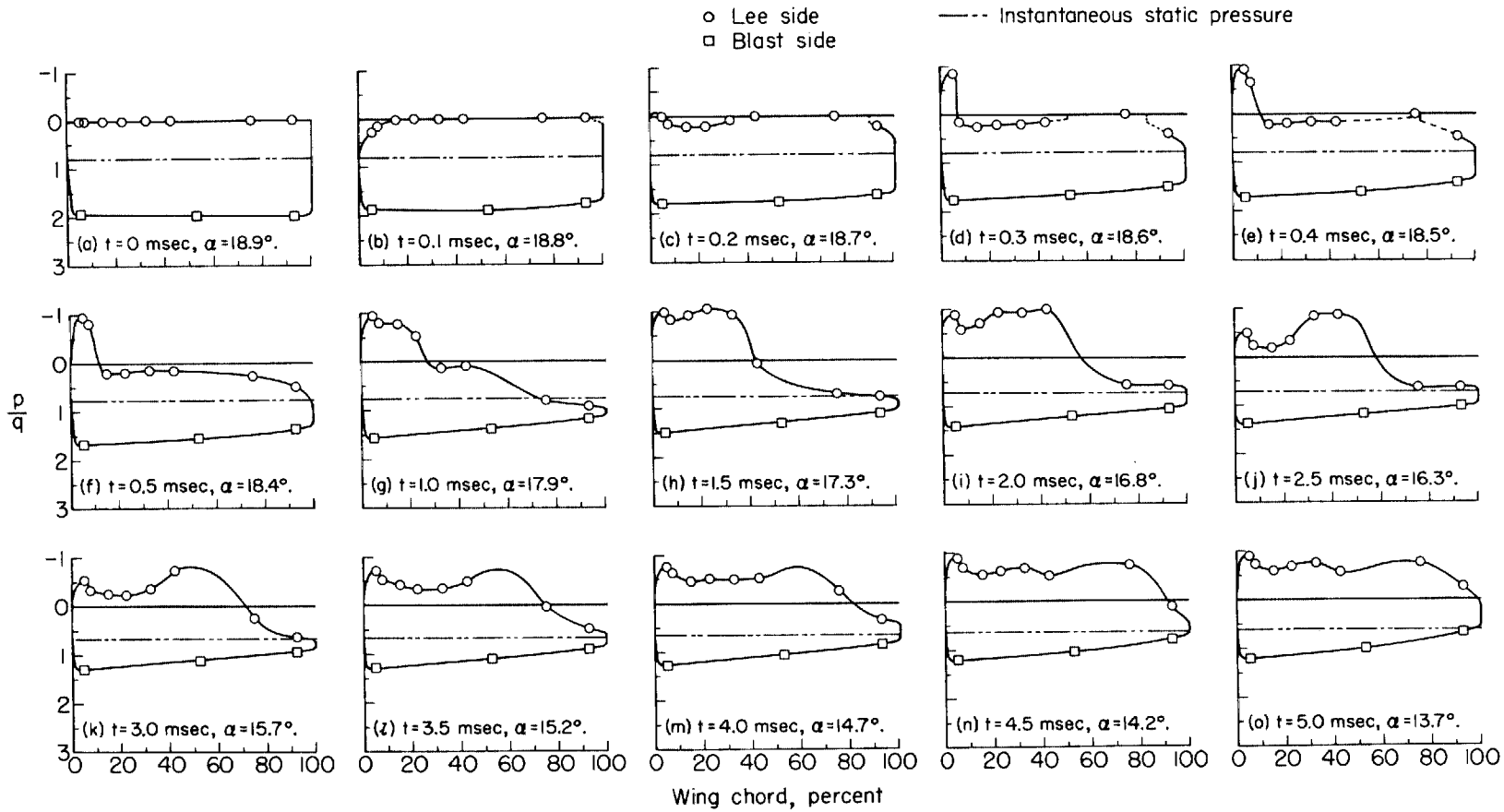

Figure 14.- Chordwise pressure distribution.

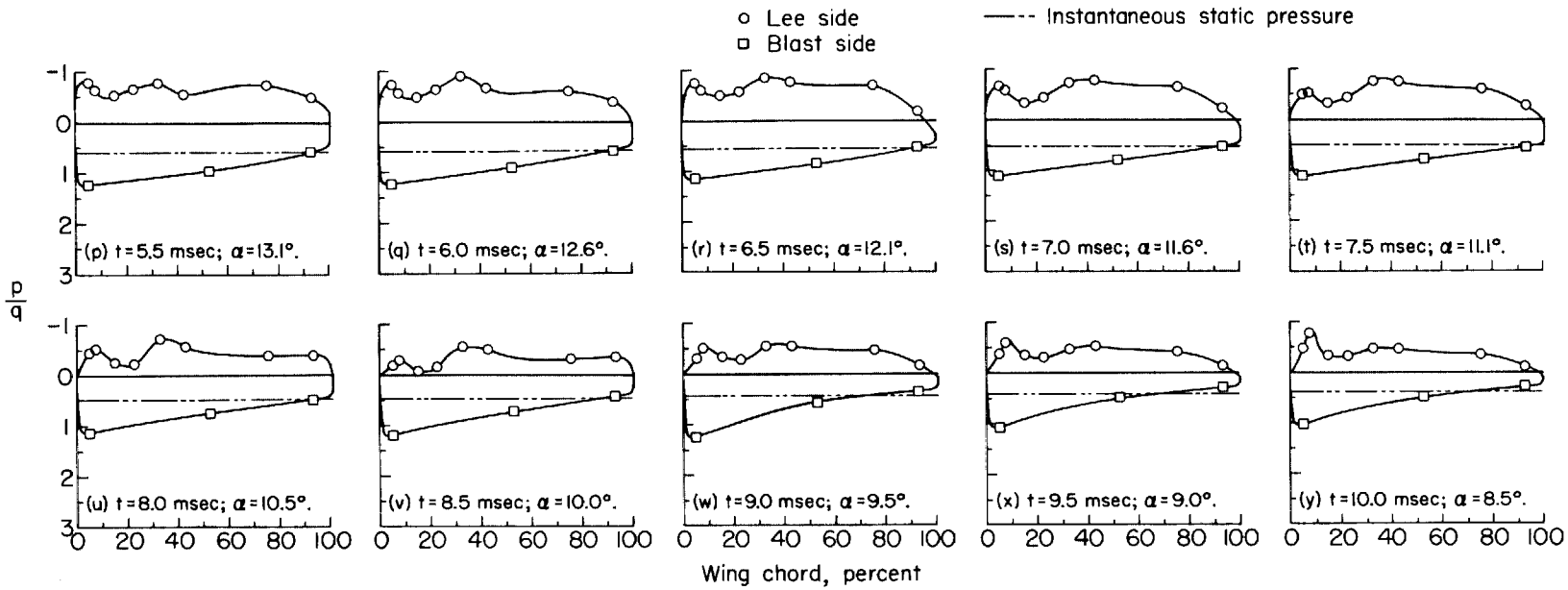

Figure 14.- Concluded.

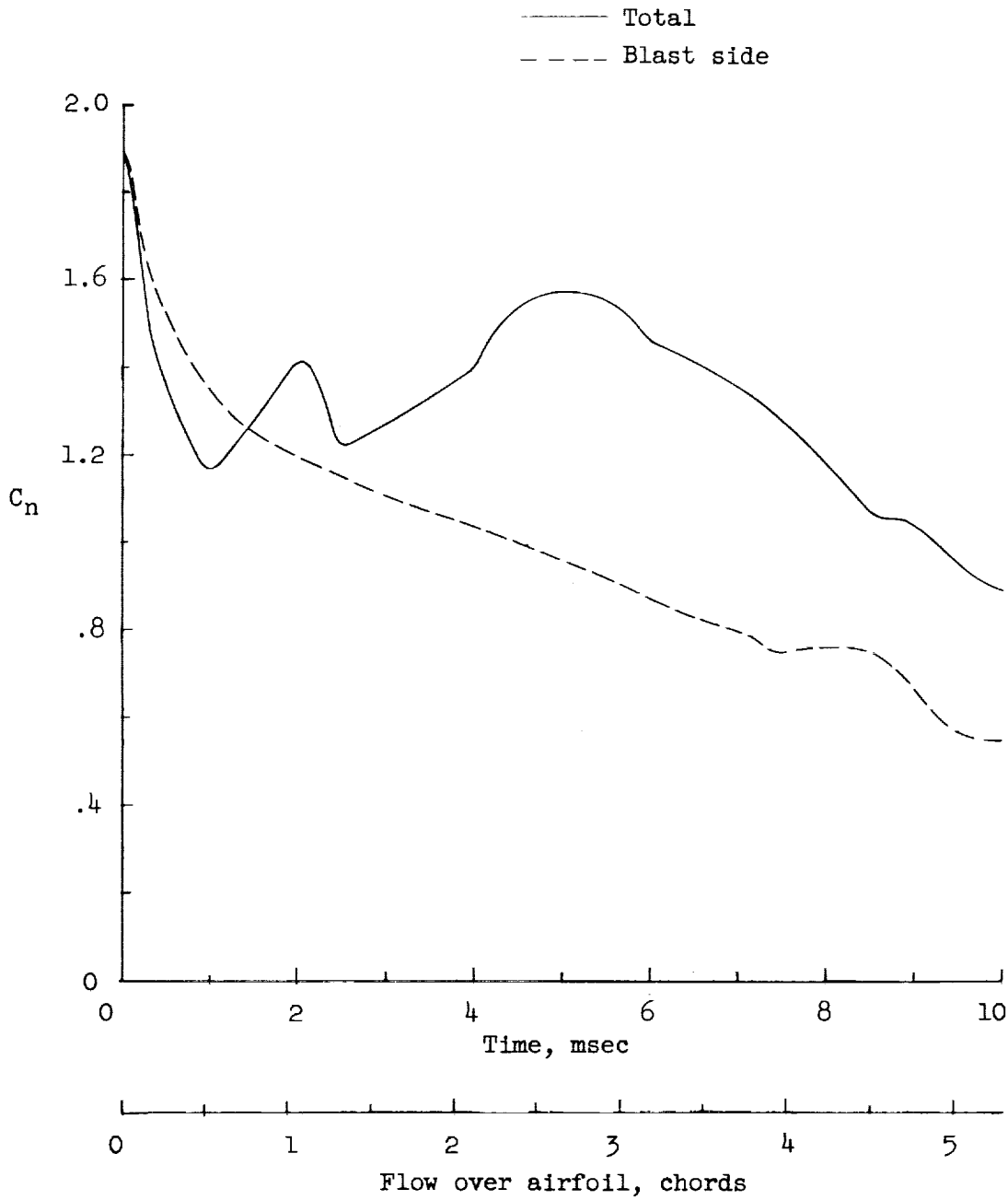

Figure 15.- History of normal-force coefficient.

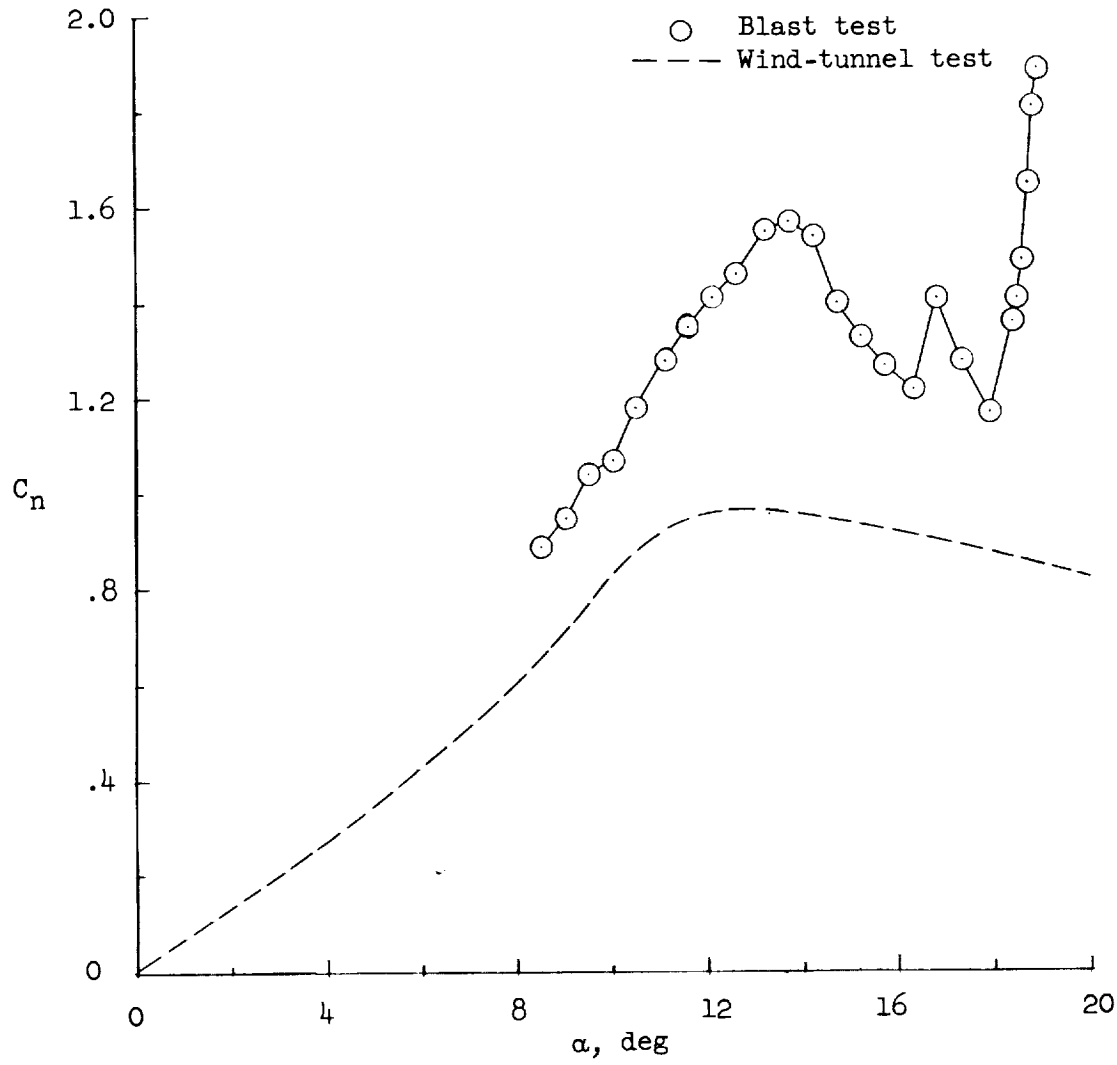

Figure 16.- Comparison of normal-force coefficients obtained from blast and wind-tunnel tests as a function of angle of attack.

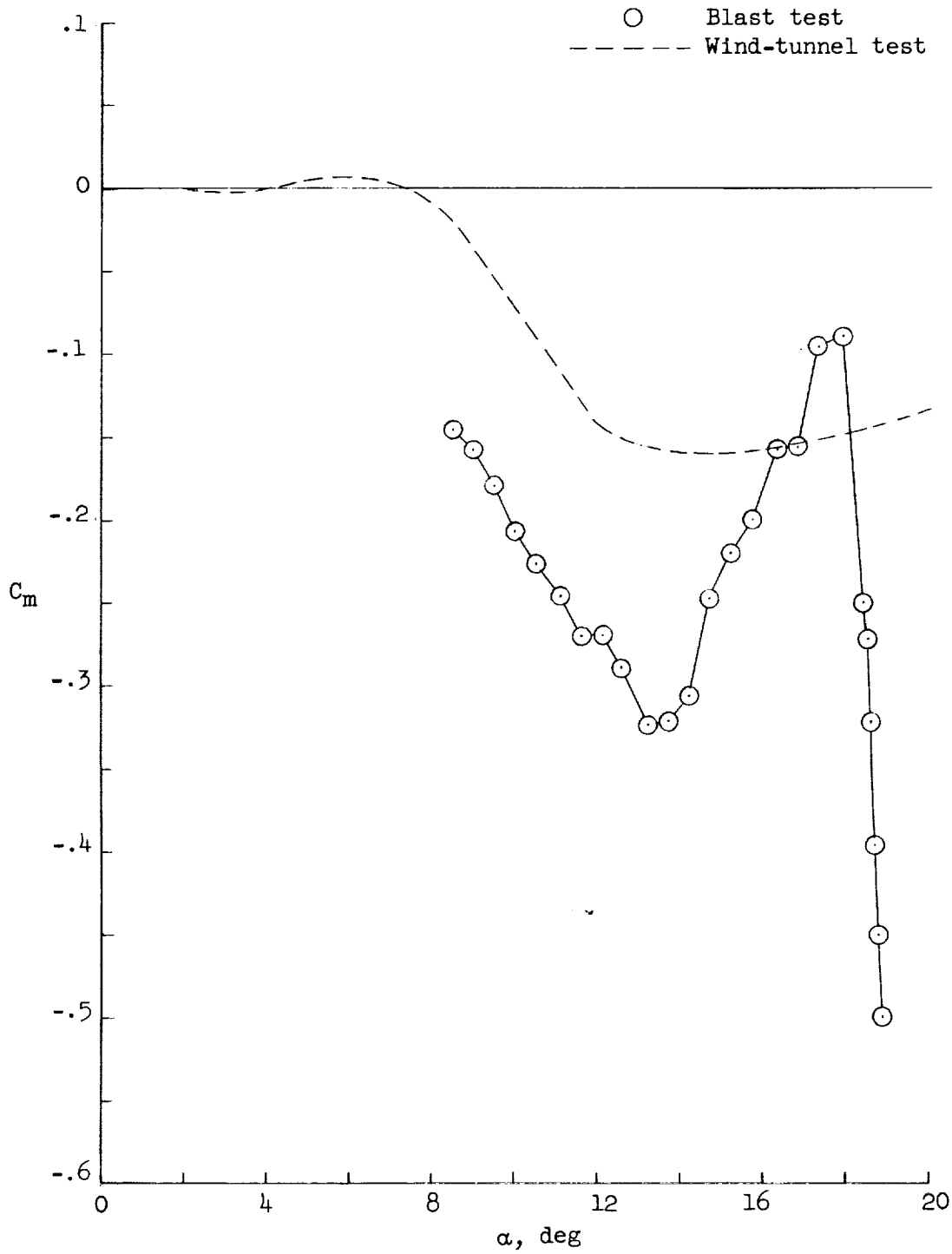

Figure 17.- Comparison of pitching-moment coefficients obtained from blast and wind-tunnel tests as a function of angle of attack.

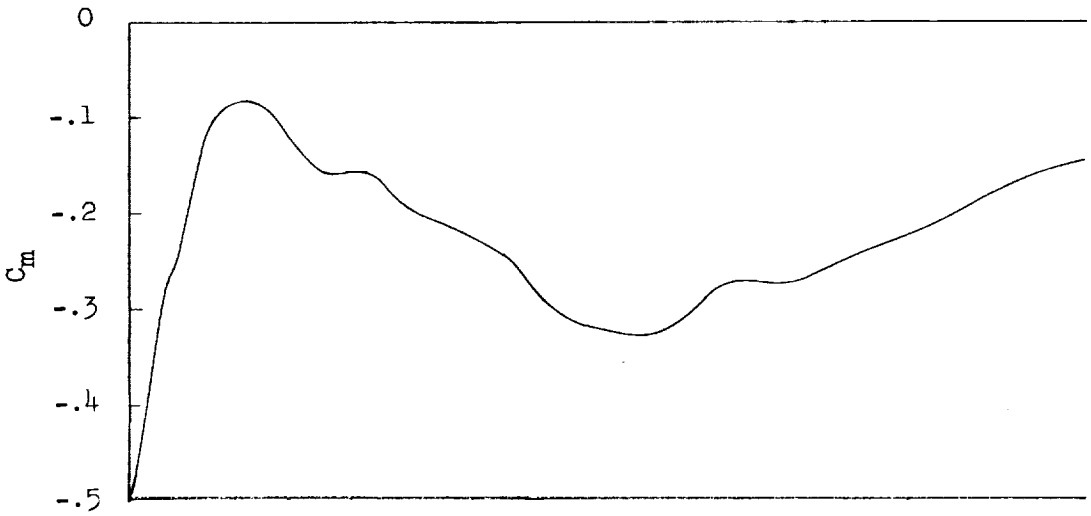

(a) Pitching-moment coefficient about quarter chord.

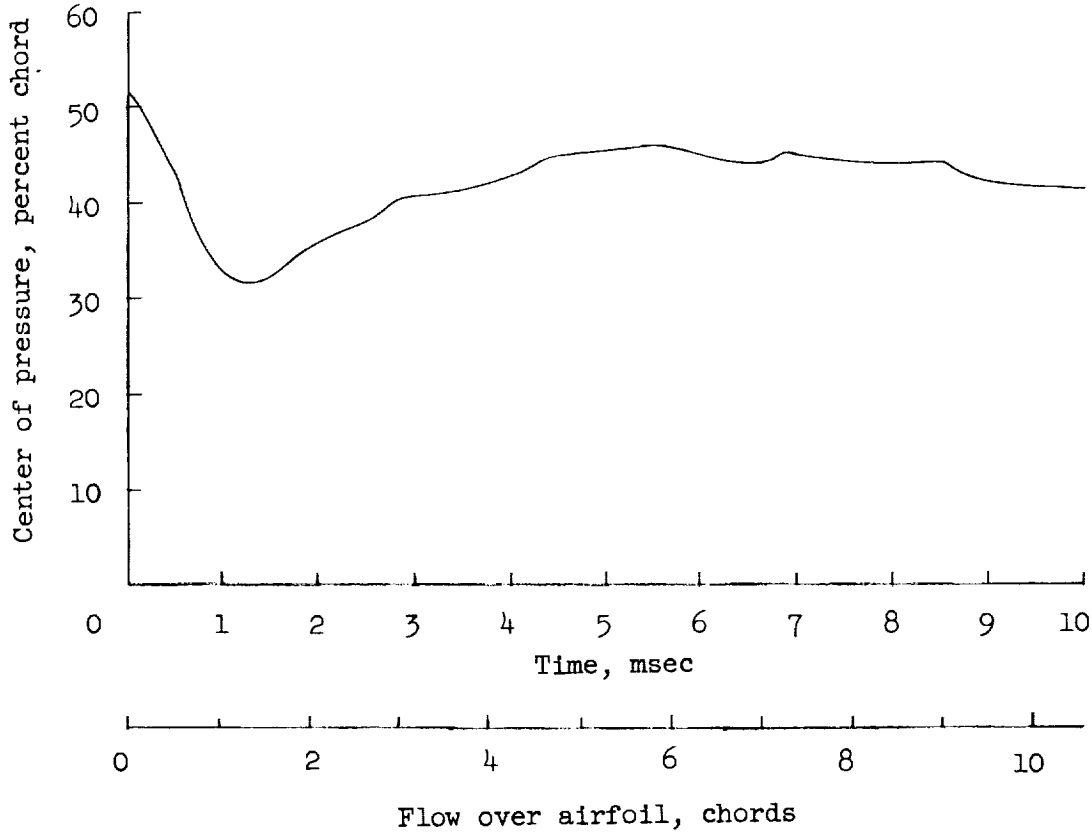

(b) Center of pressure.

Figure 18.- Time histories of center of pressure and moment coefficient about quarter chord.